Statistical Analysis of Noise From Solid Rocket Motors

Stuart A. Harper

A senior thesis submitted to the faculty of
Brigham Young University
in partial fulfillment of the requirements for the degree of

Bachelor of Science

Dr. Kent Gee, Advisor

Department of Physics and Astronomy

Brigham Young University

October 2012

ABSTRACT

Statistical Analysis of Noise From Solid Rocket Motors

Stuart A. Harper
Department of Physics and Astronomy
Bachelor of Science

A statistical analysis of noise data from various-sized solid propellant rocket motors is presented. Time waveform data sampled at 204.8kHz using 6.35mm and 3.18mm microphones were collected near motors with nozzle exit diameters ranging from 0.13m to 1.22m. Non-Gaussian features of the data are explored by calculating estimates of the probability density functions of the data, its standard deviation, its skewness, and its kurtosis. This is carried out for both the pressure waveform and its first order time difference to reveal the formation of acoustic shocks within the noise. The analysis shows greater similarity between different rocket statistics for the pressure than for the time derivative.

ACKNOWLEDGMENTS

There are many people who I wish to thank for their help and support to me in writing this thesis. First, I would like to thank Blue Ridge Research and Consulting and NASA Stennis SBIR for helping me accomplish this work. Without their generosity this work would never be accomplished.

Second, I would like to thank my advisor Dr. Kent Gee. Not only has he worked tirelessly in this field for many students including myself, but he has been a great resource and support. For almost all of the ideas presented in this thesis I give Dr. Kent Gee and his graduate students full credit. I would have never come up with these ideas on my own, and it was the patient explanations of him and his graduate students that helped me to really understand the phenomena that we are discussing here. If you have further interests in this area after reading this thesis I advise you to speak with Dr. Gee to learn more.

In the same vein I would like to thank Michael Muhlestein for inviting me to join him in his research and getting me interested in acoustics. He has been a great help to me in understanding difficult concepts, and is a great friend.

Next, I would like to thank those who have personally supported me in all of this. First in this would be my wife, Summer *The Amazing* McDermott Harper, and my children, Samuel Owen and Lynnora Lauralee. Out of anyone they have felt the burden and stress of compiling this thesis with me, and they are the strength I turn to every day. I also thank my parents and siblings for their love and support as I have studied long and hard here at BYU.

Finally, I want to thank God for all he has done for me in this, for opening my mind, answering my prayers, and giving me the energy to continue when I had none. I also thank Him for creating this amazing universe for us to discover. It still gives me great awe at His power and wisdom when I see the forces of nature in action.

Contents

List of Figures

Chapter 1

Introduction

Nonlinear acoustics is an important and growing field of study. It covers many areas of direct application including sonar and biomedical acoustics. It is inherently more difficult to deal with mathematically, and modern computing power has finally made it more assessable. Another related field of study is acoustical noise. This area of study focuses on the effects of noise and the nature of the noise itself. Often in noise analysis, because of the nearly random nature of the data, statistics becomes the tool of choice for broad understanding.

This study is a hybrid of these two fields, using statistics to understand the noise from rocket firings, which is loud enough to enter the nonlinear regime. While substantial studies exist already in rocket and jet noise statistics, this study addresses specifically how these statistics evolve in space as the noise propagates, and especially how these relate to the development of shocks in the waveform. A brief treatment on the evolution of the statistics in time will also be presented. But first some preliminary information and some motivation must be presented.

1.1   Motivation

Nonlinear acoustical noise is of great interest because it is directly applicable to our national defense and space exploration programs. One of the most noticeable effects of nonlinear high-amplitude noise is the formation of shocks (which is explained more in-depth later). These shock waves can be incredibly powerful, exerting up to 100G's each and can cause significant damage to jets, rockets, spacecraft, payloads, passengers, and launch structures. [1] [2] It is possible that these shock waves were in part to blame for the destruction of the space shuttle Columbia. While it is not known for certain it could be that these shocks blasted away some of the protective insulation on the shuttle, which it needed on reentry to prevent itself from burning up. By understanding the properties of shock formation, when they occur and why, we can better design these structures to withstand shock damage as well as to potentially save lives.

A second reason has to do with hearing loss prevention. As is discussed later, shock waves are not normally detected by conventional noise metrics. Since they can impart significant pressures to surfaces, including eardrums, and since they are hard to detect, they would go unnoticed by Occupational Safety and Health Administration standards. By understanding shocks and by finding better ways to measure them, the hearing of rocket and jet crews could be better protected.

1.2   Linear vs. nonlinear acoustics

As readers may not have extensive knowledge on nonlinear acoustics and how it leads to the creation of shocks in the wave, a brief overview on nonlinear acoustics is provided.

One of the great simplifications ever made to acoustics was the linearization of the acoustic wave equation. In order to fully appreciate this, it is important to remember that the full acoustic pressure can be expressed by the following Taylor Series:

$$p = P_0(\gamma s + \frac{1}{2}\gamma(\gamma - 1)s^2 + ...),$$

$$(1.1)$$

where P_0 is the equilibrium pressure, γ is the ratio of heat capacities, and s is the condensation ($s = (\rho - \rho_0)/\rho_0$ where ρ is the instantaneous density and ρ_0 is the equilibrium density) [3]. In order to obtain the linear wave equation, a key assumption is made that the acoustic pressure is small (or in more specific acoustical terms, that $s << |1|$). This makes it possible to ignore everything in Eq. 1.1 past the first term, and the resulting wave equation is linear.

However, when the acoustic pressure is high enough to take the second term into account (which in air is anywhere around or above OASPL 155 to 160 dB re 20μPa) then the wave equation, as well as the sound speed, becomes much more complicated. Since the wave equation is not as important to this explanation I will not derive it but instead leave that to chapter 16 of this reference [3], which does an excellent job with it, and instead focus on the sound speed.

One of the vital acoustical relationships out there is the following:

$$c^2 = (\frac{\partial p}{\partial \rho}), \tag{1.2}$$

where c is the sound speed. If I perform this differentiation on Eq. [**?**] while retaining the second term, and note that s is a function of ρ I obtain the following relation:

$$c(s) = c_0^2(1 + (\gamma - 1)s), \tag{1.3}$$

where $c(s)$ is the speed of a particular piece of condensation (and thus also pressure and particle velocity) in an acoustic wave will propagate with respect to the surrounding fluid. To get the full sound speed (c_p) it is requisite to include the surrounding particle velocity u. This leads to the next equation:

$$c_p = c_0^2(1 + (\gamma - 1)s) + u \approx c_0 + \beta u, \tag{1.4}$$

where c_0 is the linear sound speed of the medium, u is the particle velocity, and β is a dimensionless parameter of nonlinearity dependent on the medium ($\beta = (\gamma + 1)/2$) [3]. For air $\beta = 1.2$, and thus is small enough that nonlinear effects are not noticed until about 155 dB to 160 dB is reached. One of the great effects of this is seen in Figs. 1.1 and 1.2, where because the peaks in the wave have a
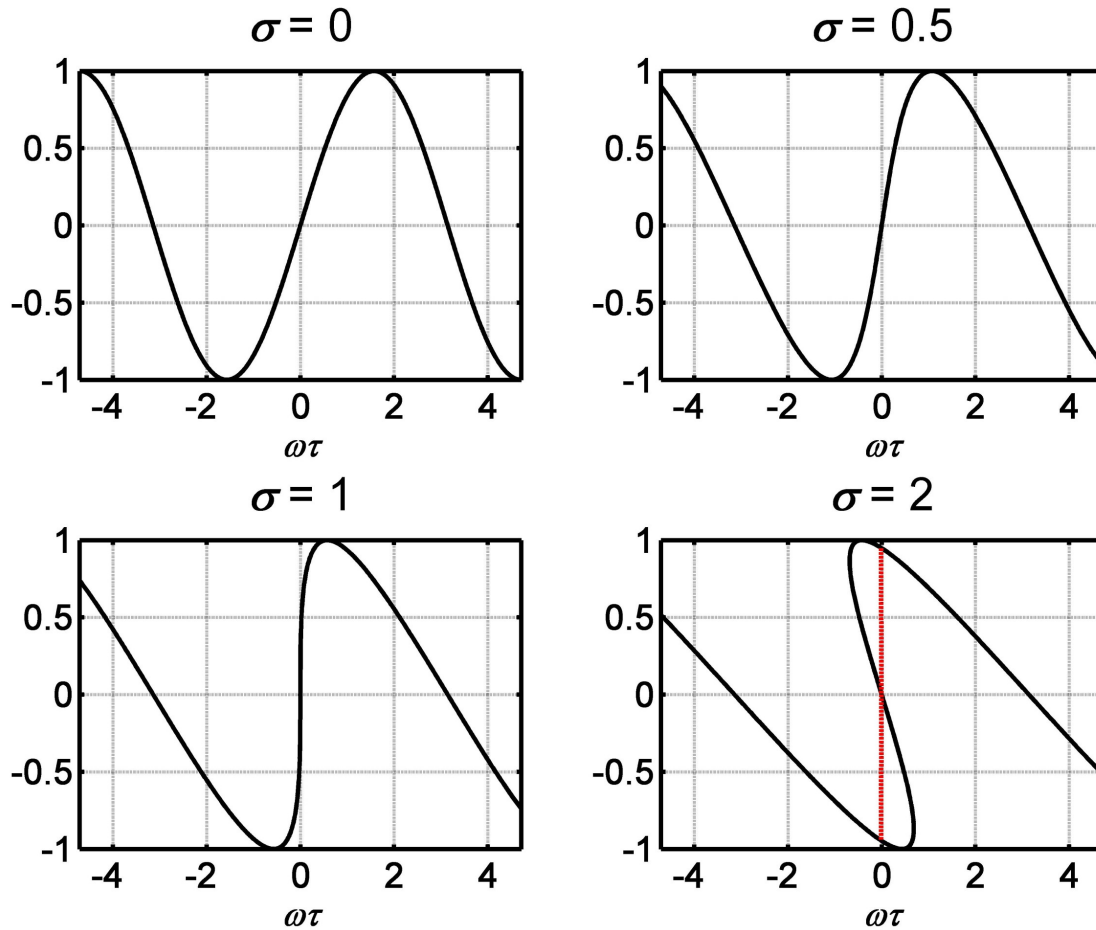
Figure 1.1 In the first frame the wave begins as a perfect sine wave with high amplitude. Note that the x axis is in retarded time(σ), which means that we are looking at and following the same piece of the wave as it propagates to the left at speed c_0. As the wave propagates the compressed part of the wave, or the peak, travels faster than the rarefaction. When $\sigma = 1$ we have reached what is called the shock formation distance. After this point the overlap is handled by weak shock theory to create a sawtooth wave. [4]

greater *s* they move faster than the troughs and eventually a sawtooth wave can be formed from a sine wave.

This effect is called an amplitude dependent sound speed, which means that the higher the particle velocity is (or in other words the higher the pressure) the faster the sound moves. Though it can be derived mathematically, it still can be hard to grasp. Hence, it is important to look at it
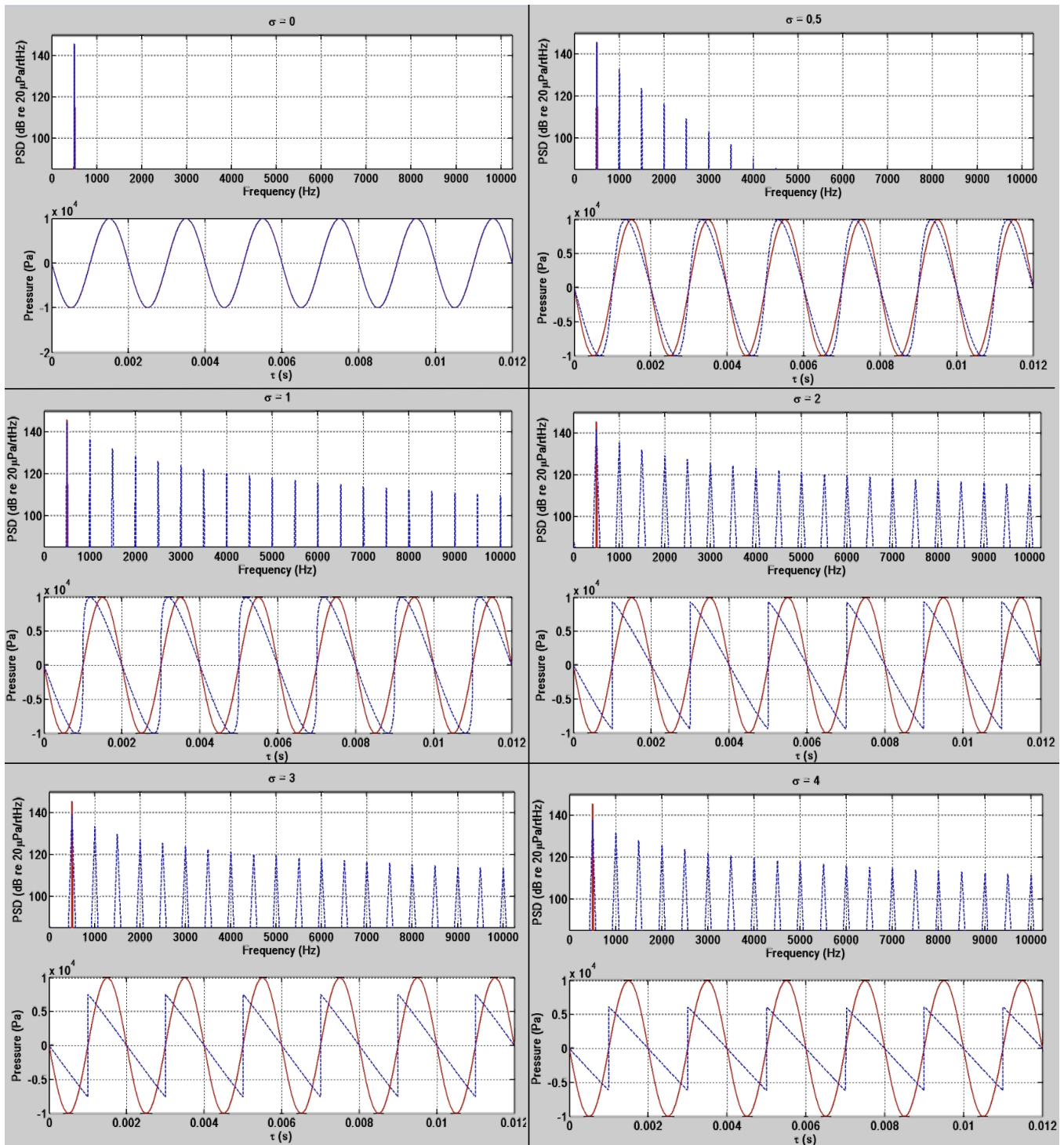
Figure 1.2 As a nonlinearly propagating sine wave travels in space it begins to distort. This distortion causes its spectral energy distribution to no longer be a delta function, but instead the energy pumped into higher frequencies. This effect causes a fast nonlinear decay in the sound amplitude, even when there is no absorbtion which can be seen as the wave propagates.

from a different angle to get more of a conceptual grasp as to why this occurs.

Sound wave compressions are adiabatic due to their quick speed, and thus they fluctuate in temperature. Now, it is a well-known property that temperature, even in the linear regime, can affect the overall sound speed. In small amplitude waves the temperature fluctuations caused by the adiabatic wave compressions are so small that they are negligible and do not affect the sound speed. But once a certain level of sound is reached (which again is around 155 dB re 20μPa) the hotter, more compressed areas of the wave move faster than the colder, more expanded areas.

With a firmer grasp on these ideas it is now possible to proceed to the inevitable conclusion of an amplitude dependent sound speed. Imagine that we have a sine wave similar to the ones in Figs. 1.1 and 1.2, and imagine that I am following a particular piece of the wave as it propagates along at c_0 [this is called "retarded time" (σ)]. As the peaks begin to overtake the troughs, the line between them becomes steeper and steeper. Eventually it reaches a point of infinite slope, its first shock. This point is called the shock formation distance ($x = c_0/(k\beta|\vec{u}|)$ or $\sigma = 1$).

As I continue following the wave downstream, the mathematics begins to dictate that the wave would be multi-valued. This is unphysical for a pressure wave, and a new model is required to solve this problem. This model is called weak-shock theory. The wave is approximated by drawing a line that makes equal area on both sides. The result is the eventual transformation of a sine wave into a sawtooth wave [4]. Though this is not a perfect model it does work incredibly well in practice with minor adjustments. When this is nested inside of nonlinear noise the result is an audible popping or crackling effect in the sound anywhere farther downstream than $\sigma = 1$. These are the shock waves referred to in the motivation, and are often referred to collectively as "crackle."

Note that the example given in Figs. 1.1 and 1.2 are in a lossless environment; yet, upon close inspection of the last few frames the wave is losing amplitude. This is an effect known as nonlinear absorption. It arises from the fact that as the peek further laps the trough the line that separates the two areas of equal area, and hence that line becomes shorter and shorter. This causes the amplitude

of shocks to die out quickly. This is an important effect that will come up later in this work.

Another effect of shock formation is the pumping of energy into higher frequencies. This effect can be seen in Fig. 1.2. For example the spectrum of a sine wave is a delta function. But if the sine wave developed shocks the hight of the original delta function would decrease and a vast array of smaller delta spikes higher in frequency would form as it became a sawtooth wave. Thus energy would be transferred from one frequency into another.

Now in real life do shocks really form a perfect sawtooth wave? The answer to that is no. There is no such thing as a perfect discontinuity in a physical sound wave, and there are some rounding effects due to atmospheric absorbtion. However, as stated earlier, this model does work very well and does help us reach some important conclusions.

1.3   Statistics as a tool to understanding nonlinear acoustic noise

The next level of difficulty is to change the source of nonlinearity from a discrete signal to random noise. Once this level of complexity is reached the math needed to predict the wave's generation and propagation become near impossible to compute, especially when the source is extended like a rocket plume. It is noted from observations of nonlinear noise, like the sample seen in Fig. 1.3 that the principles of shock formation discussed above still hold. However, because of the random nature of noise (particularly rocket noise in this study) statistics becomes one of the best tools to analyze the the sound. There are several measures that are especially useful that need some further explanation.

However, before discussing these statistical measurements there should be a brief note made. In the above section σ was used in connection with retarded time based off of shock formation distance. This worked well for discrete signals. But in noise there is no unified shock formation distance due to differing initial peak amplitudes. Taller peaks simply form into shocks faster than
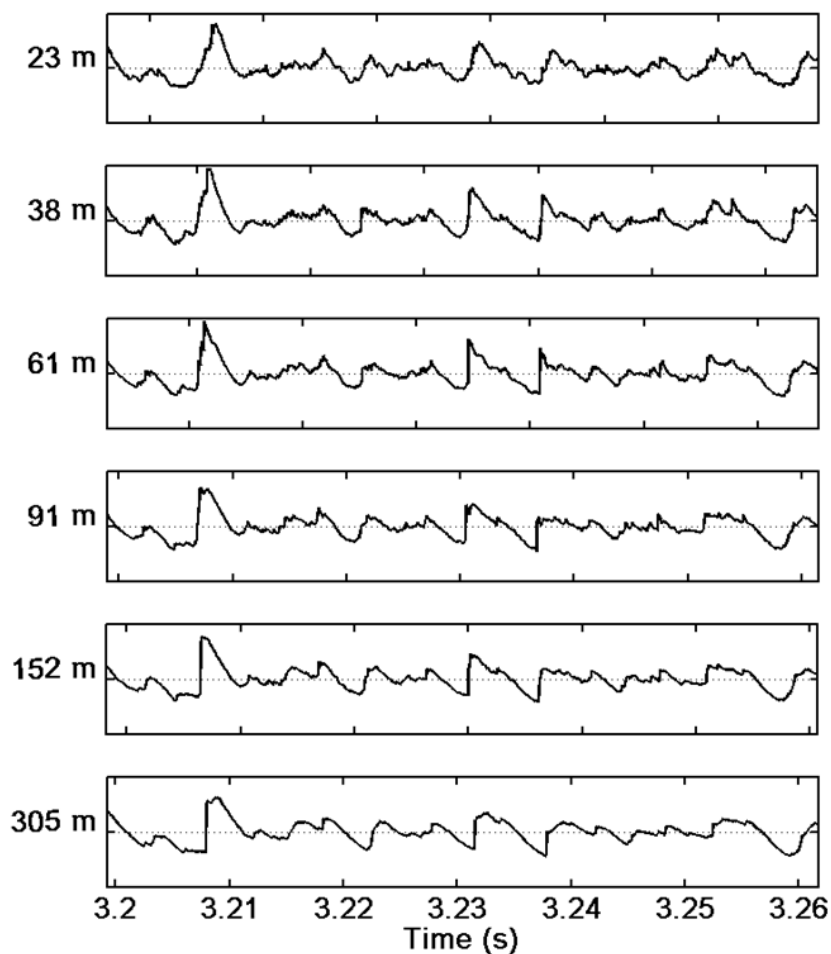
Figure 1.3 This recording is a comparison of noise from the F-22 Raptor from progressing locations. Note how there is no unified shock formation distance, but that it occurs faster for the louder peaks than the smaller peaks. This noise by $d =$61 to 91m sounds very "crackly." (Note that though the x-axis says "Time (s)" it should say "Retarded Time (s).") [5]

the smaller ones. Hence retarded time will no longer be useful. Unfortunately, an important statistical measurement, standard deviation, also, uses the symbol σ. From this point on in the thesis σ will refer to standard deviation and not shock formation distance.

1.3.1 Standard deviation

The first statistical measurement discussed, and probably the most familiar to physics students, is standard deviation. The standard deviation describes how scattered a particular distribution is. In acoustics it is used to calculate the average amplitude of a sound wave. The standard deviation of the wave is equivalent to the root mean square (RMS) pressure if the wave has a mean of zero, and can be used in the following equation to find the overall sound pressure level (OASPL):

$$OASPL = 20\log_{10}(p_{rms}/p_{ref}),\tag{1.5}$$

where p_{rms} is the RMS pressure and p_{ref} is a reference pressure, which is most commonly 20μPa.

When it comes to nonlinear noise though, and finding shocks in the wave, I find that standard deviation and OASPL are not incredibly insightful. These quantities simply do not reveal a strong correlation between the presence or absence of shocks [6]. They may say that the conditions are right for them to form, but because they happen so fast their significant amplitude does little to affect the overall RMS pressure.

Though standard deviation in and of itself is not hugely insightful, there is one thing that I will be using the standard deviation for quite extensively in this work, which will be seen in the next section.

1.3.2 Probability density function

Probably the most widely explored statistical measure in this study is the probability density function (PDF). For those who are unfamiliar with it, it is similar to a histogram or a $|\Psi|^2$ function

in quantum mechanics. It describes the probability that a certain function or wave will contain a particular given value. For an acoustic wave, a PDF describes the probability of finding a particular pressure. The equation to create a PDF is a difficult one and does not work well for a discrete data set, like a recording. Another way to make a PDF is to create a histogram of the noise. The histogram approach is not a perfect way to create a PDF, but it is very useful because it is easy to do on a data set or recording. For my PDF's I divided the pressures into 91 evenly spaced bins. Note that in order to get a smooth PDF function from discrete data the appropriate number of bins must be chosen. If the binwidth is too small from having too many bins, it looks like a sloppy array of small spikes. If there are too few bins then there is not enough resolution. Thus my PDF's do exhibit some roughness simply because the nature of the problem, but I found that for the most part 91 bins smoothed things well enough. Then to make them all comparable I normalized them by σ. The equation to accomplish this is given here:

$$PDF(x/\sigma) = \frac{Histogram(p(t))}{\sigma(\delta w)n}, \tag{1.6}$$

where $p(t)$ is the pressure wave in time, σ is standard deviation, δw is the distance between each bin, and n is the number of samples in the wave. Hence, any changes in the shape of a PDF do not come from amplitude changes, but instead come from physical changes in how the sound is distributed. This method of normalization is reminiscent of the process that many acousticians use to collapse the spectra of different rockets by their peak frequency as a means to compare multiple rocket spectra.

Most random noise has a PDF with a Gaussian shape or very close to it. Thus the rocket and jet noise PDF's will be compared to a standard Gaussian distribution. A jet noise PDF is shown in Fig. 1.4 as a sample. This particular recording shows a very strange shape, which is similar to, but not Gaussian. This shape, as discussed latter, is also found in rocket noise statistics.

Ffowcs Williams, et al. in their 1975 ground-breaking work on jet noise, used the PDF to analyze the content of jet noise [6], and since then it has been used widely in that field. This is due
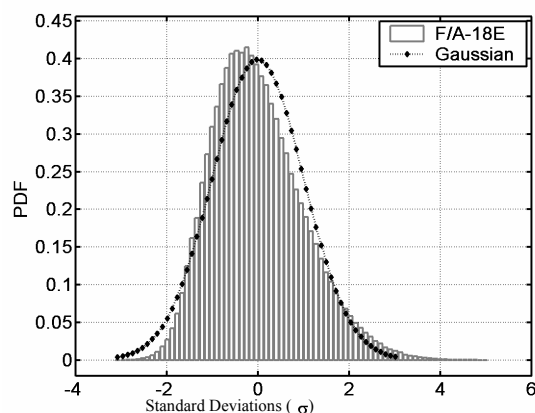
Figure 1.4 PDF of an F/A-18E at afterburner compared to a Gaussian distribution [5]. This is a fine example of a continuous PDF (the Gaussian) and a PDF comprised of discreet data points (the PDF of the rocket noise).

in part from the fact that many statistical measurements that are considered noteworthy in this field are derivable from the PDF of the noise. These statistical measures each tell an important story concerning the way the data is distributed. The measures of interest are standard deviation (which has been already covered), skewness, and kurtosis. These will be covered in full in the next two sections. Another thing that Ffowcs Williams, et al. did was to plot the x axis of their PDF's with respect to standard deviation as was discussed earlier in Fig. 1.5. Though this standardized scaling has not been followed by every researcher in this field, most have traditionally (and thankfully) done this.

Now a downside to the PDF is that as a 2D line graph it is only able to show the statistics for one position. However, I will explain in Chapter 2 a graphical representation that Dr. Gee and myself have developed on how show this statistical measurement evolves in space.
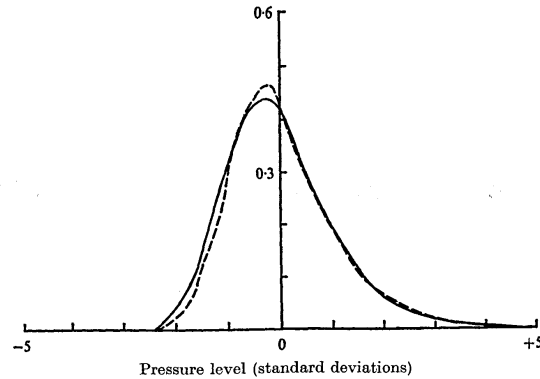
Figure 1.5 A PDF of the Olympus 592 engine and a 1:10 scale model (the model is the dashed line). Note how similar they are when they are compared not by raw amplitude but instead by standard deviation [6].

1.3.3 Skewness

The next statistical measurement that is needed is skewness. It is a measure of how asymmetric a distribution is. Mathematically the definition of skewness is as follows:

$$Skewness = \frac{\sqrt{n(n-1)}}{n-2} \frac{\frac{1}{n}\sum_{i=1}^{n}(x_i - \bar{x})^3}{(\frac{1}{n}\sum_{i=1}^{n}(x_i - \bar{x})^2)^{3/2}}, \tag{1.7}$$

where n is the number of samples in the distribution and $\bar{x}$ is the mean average of the distribution. in my anaysis I used the standard, built-in MATLAB skewness function. For example, for a roughly Gaussian distribution of numbers the distribution would be symmetric and the skewness would be zero. If a relatively small number of values was added to the distribution compared to the total number, but they were all five or six standard deviations out, then a positive skew would result. An example of this is given in Fig. 1.6.

Skewness was also first employed as a measure of nonlinearity by Ffowcs Williams, et al. in their 1975 paper [6], and was asserted to be the defining characteristic that would determine wether or not the sound wave contained crackle. Their general rule that a skewness at or above 0.4 that the noise crackles strongly seems to hold in most situations, and it makes sense since shocks tend to be higher in amplitude than the surrounding noise. But their claim was disproved as a sure measure of

Negative Skew   Positive Skew
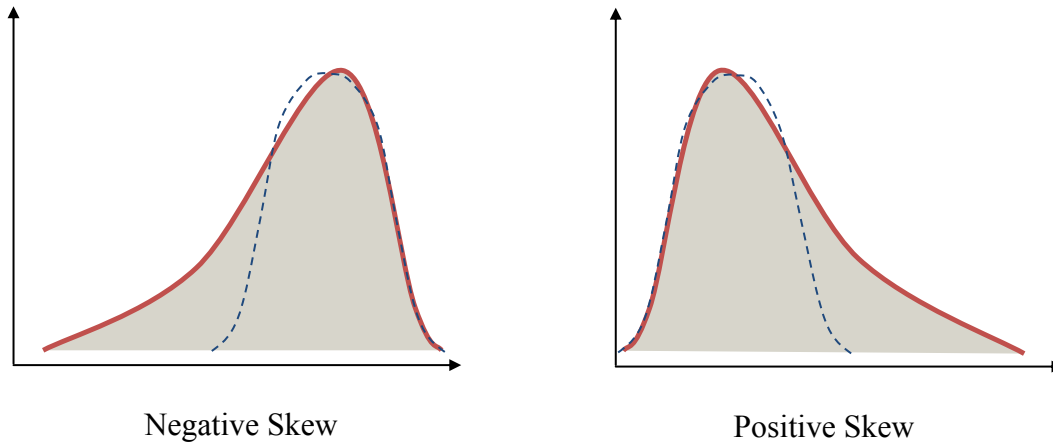
Figure 1.6 An explanation of what kind of distribution creates positive or negative skewness.

shock content as Gee, et al. were able to create a waveform with all the necessary statistics set forth by Ffowcs Williams, et al. but yet was crackle free [5]. Another problem with relying on skewness is the effect of nonlinear absorbtion can lower shock values till the skewness will drop beneath 0.4, even tough there are still shocks. However, I still use it as a statistical measure because it is still insightful in normal situations.

1.3.4 Kurtosis

The final statistical moment in this study is kurtosis. This one has not received as much attention in the jet and rocket noise field, but it is still useful as a way to measure shock content. Kurtosis measures how peaked a particular distribution is compared to the outliers. Mathematically, its definition is:

$$Kurtosis = \frac{\frac{1}{n}\sum_{i=1}^{n}(x_i - \bar{x})^4}{(\frac{1}{n}\sum_{i=1}^{n}(x_i - \bar{x})^2)^2}. \tag{1.8}$$

The more outliers farther out compared to a high central peak on the PDF, the greater the kurtosis. For a uniform distribution the kurtosis is one, for a Gaussian distribution it is three. To calculate

this I have simply used the built in MATLAB kurtosis function.

1.3.5   Time derivative of the noise

Even with all the previous statistical moments it is still not sufficient to analyze this data for shock content. These methods, though helpful, are limited and with them there is no sure way to know if shocks are truly present [5]. And other statistical moments have been shown to reveal nothing more than the ones already discussed concerning the nature of the data [7].

In order to solve this problem McInerny, et al. [8], Petitjean, et al. [9], and Gee, et al. [5] have explored the possibility of measuring shocks by using the "time gradient" of the wave, or better known as the time derivative. This method has the remarkable potential to detect even the smallest amplitude shocks because it catches the nearly infinite slope that characterize them. An example of this is seen in Fig. 1.7. In this figure the same time segment of noise is shown, but the first shows the pressure, the second shows the time derivative. And where before it had been difficult to identify where the shocks were, in the second it is easy to see where they are occurring.

It is also possible apply the exact same statistical tools to the first order time derivative. This opens up new possibilities for analysis. Theoretically, if these waves were random Gaussian noise, than the PDF of the time derivative would also have a Gaussian distribution. If major differences are observed, particularly a comparatively small number of enormous values, then nonlinear propagation and the presence of shocks can be inferred.

1.4   My purpose in this research

This research expands on the work done by the others mentioned previously by expanding the statistical analysis in new ways. Noise data were taken at dozens of positions in the near and far field of three different sized rocket motors. The statistics were evaluated at each position for the
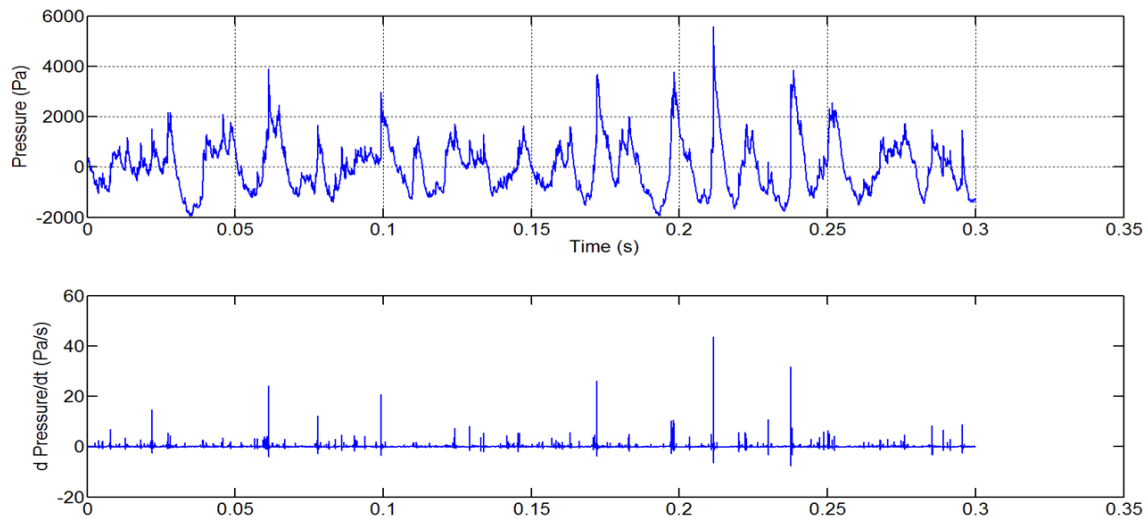
Figure 1.7 The first graph in this frame is a section of data from the GEM 60 Rocket. Shocks are evidently present through observation, but may or may not be evident by any statistical measures. But in the first time derivative, as shown in the second graph, the location of shocks are incredibly evident visibly and statistically.

data and its time derivative. With this information it is now posible analyze how the statistics evolve in space, how the statistics are related to rocket size, and how the statistics are related to shock formation.

Chapter 2

Experiment Summary

2.1   Rocket information and recording layout

First and foremost it is important look at how the rocket noise was recorded from each of the three rockets and how locations have been scaled to make them more comparable. Each of these rockets were recorded with differing microphone equipment, layout, and orientations. If the results are to make any sense these differences must be understood. Aspects not covered here can be found in 'Appendix A: Rocket Information.' (Note that each of these rockets use similar solid rocket propellant that is used in the pace shuttle's Reusable Solid Rocket Motor (RSRM).)

    Each of these tests used a wide variety of probes and microphones. Many of these probes were designed to record the sound with multiple microphone orientations in order to determine the direction of sound propagation and fluid motion. However, the statistical properties of the sound are scalar quantities and are not direction dependent, thus at these locations only one of the microphones were used, with preference given to those microphones that were pointing vertically. This preference allowed for optimal statistical recordings as these microphones are designed to be most accurate when the sound approaches at grazing incidence.

2.1.1   5 inch CP

The first and smallest of the rockets is the 5 inch (12.7cm) CP. The recordings were taken August 22nd 2008 at ATK Space Systems' small motor test facility in Promontory, Utah [10]. This rocket has, as the name implies, a rocket nozzle that is five inches in diameter and was filled with seven pounds of solid rocket propellent. Each burn lasts about 2.5s. The rocket was positioned horizontally such that the motor axis was 81cm above the ground.

This set of recordings was unique compared to the other rocket recordings in that this was not a single rocket firing. Instead recordings were taken over the course of 32 different firings. There was rig of four tetrahedral probes set along a line that was 12° off of the center axis and six inches displaced. after two firings, the rig would be moved along this line for another set of recordings. Three stationary microphones were also set in place to make sure that the spectrum and statistics between each firing were consistent. This method made it possible to have two lines of eighteen recordings that run 12° off the center axis, referred to as 5in CP test line 1 and 2 respectively. The relatively shallow shear layer angle as well as the proximity was only possible due to the smaller size of the rocket. Rockets of larger size require that the microphones run along a line that is 16° to 22° from the center axis to prevent damage to the microphones. In Figs. 2.1 and 2.2 the layout and equipment are displayed graphicly. The first out of the two figures shows the test rig, a close up of one of the spherical probes, and the stationary microphones (not included in this analysis) next to the rocket plume. The second figure gives the location of the test rig with respect to the rocket over the several tests.

2.1.2   Orion 50

The second rocket in this study is the ORION 50, a rocket that has been used on the Pegasus and Taurus vehicles. This test took place on June 24th, 2010 at the T-6 ATK test facility near Promontory, Utah. The rocket has a 3ft (91.44cm) diameter nozzle which is vectorable. For this
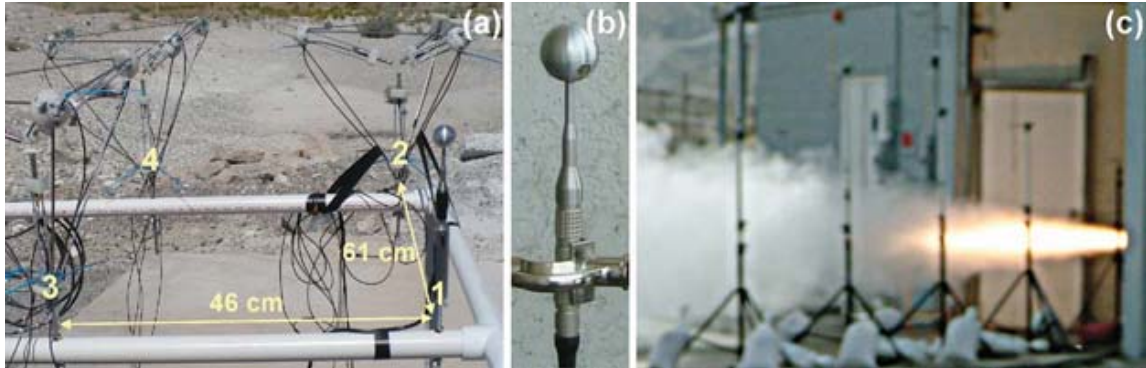
Figure 2.1 a) The probe rig that was used and its general orientation to the rocket. b) The NASA spherical probes. c) The stationary microphones in relation to the 5in CP test [10]. The different probe types will be addressed latter.
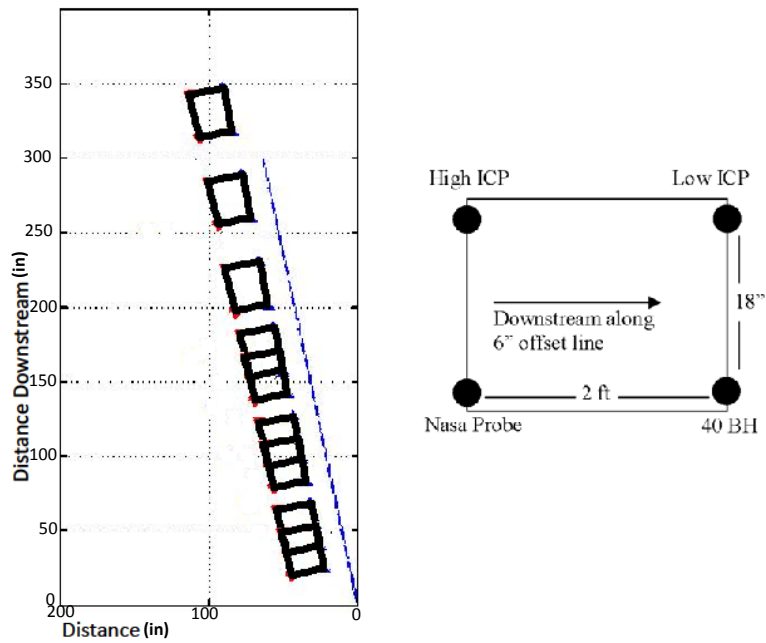
Figure 2.2 The basic rig layout and how it was moved with relation do the motor. The maximum distance downstream it was moved was 240 inches.
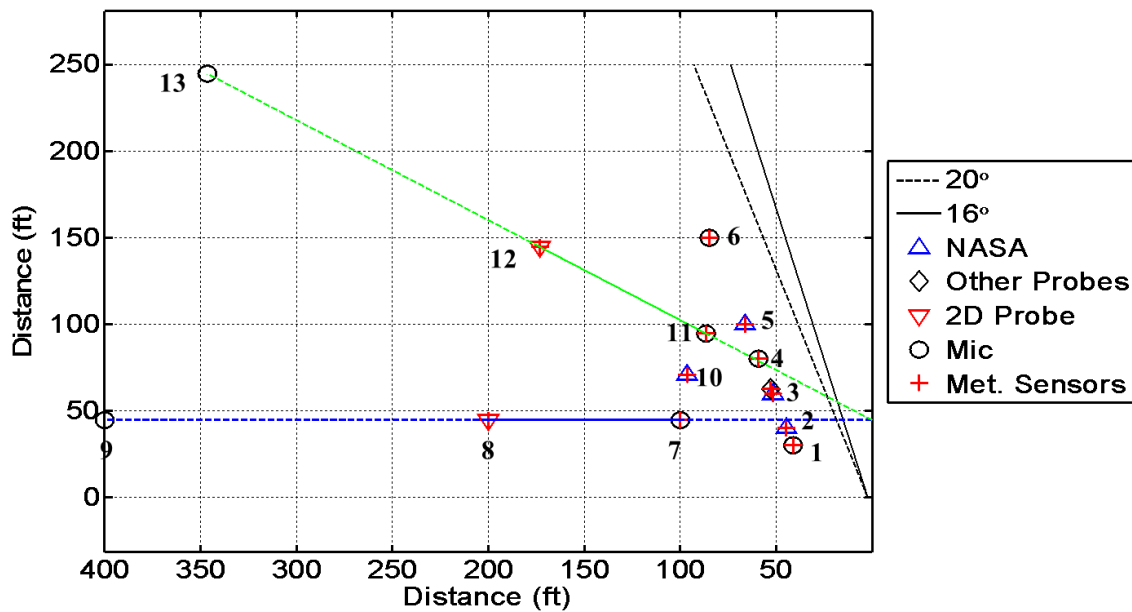
Figure 2.3 The layout of the microphones for the Orion 50 test. The meaning of the numbering is given in Appendix A

test the nozzle was gimballed. Much of my statistical analysis ignores this, but it can potentially be an important factor in the time evolution of the statistics.

The microphones for this test were set along three major lines. The first is set along the plume 20° from the rocket axis and consists of six microphones. The second is set 60° from the the rocket axis and consists of four microphones. The third line was set 90° from the rocket axis and also consisted of four microphones. These lines will be referred to as the ORION shear layer, 60° radial, and 90° radial respectively. For a graphical representation of these tests, see Figs. 2.3 and 2.4. The first figure shows the layout of the microphones, what kind of probe was placed at those locations, and the lines delineating where the plume is located. The second is a picture of the test site. Off to the left is the rocket nozzle and across the middle there are several tripods with microphones and probes.

Figure 2.4 The microphone layout that was used in the Orion 50 test and its general orientation to the rocket.

2.1.3 GEM 60

The final rocket in this study is the GEM 60, a 4ft (1.22m) diameter nozzle rocket that is used on the Delta IV Medium launch vehicle. This test was taken on the 19th of February 2009 at the ATK T-6 test facility near Promontory, Utah. During this test the nozzle was held fixed. Total burn length lasted approximately 90s where the significant thrust portion of the burn is only 85s [11].

The microphones were set along three major lines. The first, like the ORION 50, is set along the plume 20° from the rocket axis and consists of ten microphones. The second line is set 60° from the center axis and consists of four microphones. The last also consists of four microphones and is set 70° from the center axis. These three lines will be referred to as the GEM shear layer, 60° radial, and 70° radial respectively. For a graphical representation of these tests, see Figs. 2.5 and 2.6.Again, the first figure shows the layout of the microphones, what kind of probe was placed at those locations, and the lines delineating where the plume is located. The second is a picture of the test site, which happens to be the same place as before. In the center is the rocket nozzle,
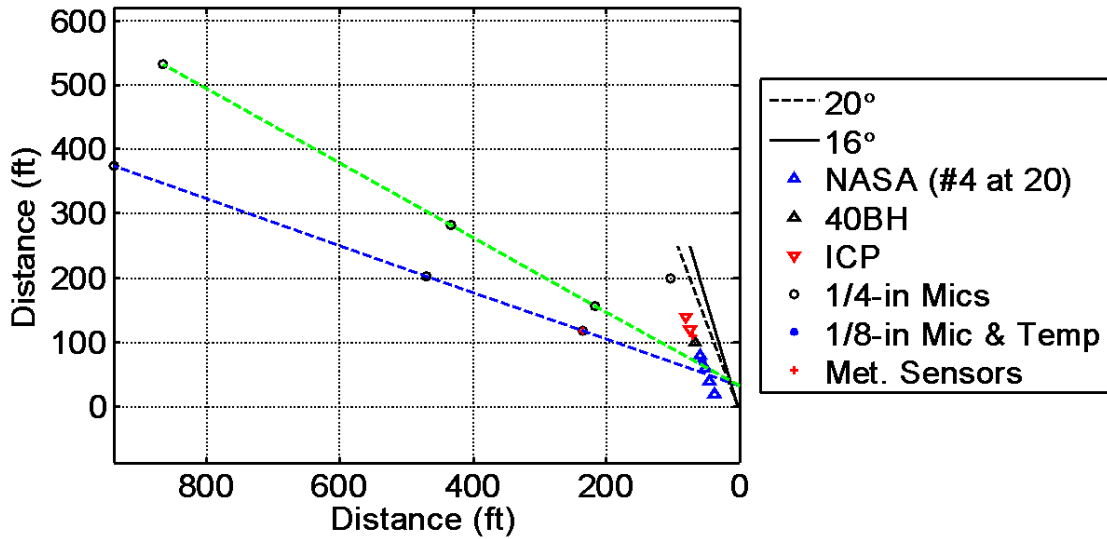
Figure 2.5 The layout of the microphones for the GEM 60 test.

Figure 2.6 The microphone layout that was used for the GEM 60 test and its general orientation to the rocket.

which is barely visible, and stretching from the building to the camera there are several tripods with microphones and probes.

There is one issue of concern with the GEM-60 data. I have compared some of my work with the work done by Gee et al. [11] and I find major discrepancies in the OASPL graphs that he made and that I made (See Appendix A for the graphs) I can find no error in my code, but yet I know that my version cannot be correct since the sound level is jagged as we go downstream. The values in the far field (>30D) correlate to Gee's graph, but before that point they fall below what Gee et al. put forward. Hence his graph is included because I believe it is more accurate than my own. I have also been assured by Dr. Gee that this will not have any significant effect the statistics, especially the PDF's, since they are already normalized by the standard deviation. However, I feel it important to make the reader aware that there may be flaws in his work that could be resolved in the future.

2.1.4 Normalizing and comparing distances

In order to compare these recordings some normalization is necessary. Because the power of each of these rockets some microphones had to be placed farther out than others. To do a scaled comparison, it is vital to scale the distance by the size of the rocket, otherwise the comparisons would have no meaning. Thus all distances are normalized by nozzle diameter. This is a common practice in rocket noise acoustics.

As can be observed in Figs. 2.7 and 2.8, the lines of microphones are now much closer together and can be compared with greater ease. The radials are still a little difficult to compare, but that is not a major issue to this research. Though this may help scale and compare these rockets it still is important to keep the true dimensions in the back of our mind, or else my arguments regarding the effect that the power of each rocket on the acoustics will not make sense.
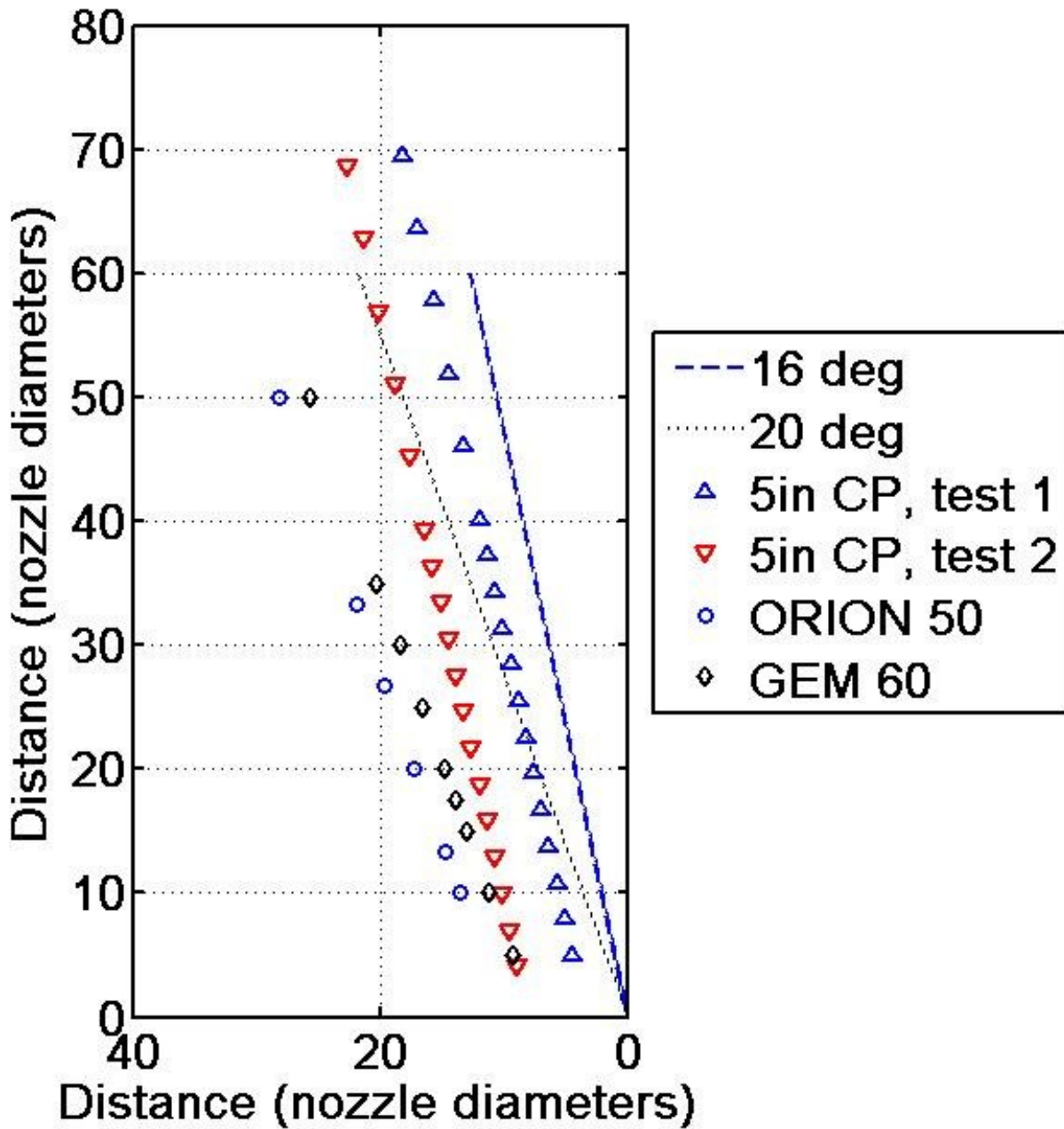
Figure 2.7 The combined layout of all of the microphones in the near field, having been normalized by nozzle diameter.
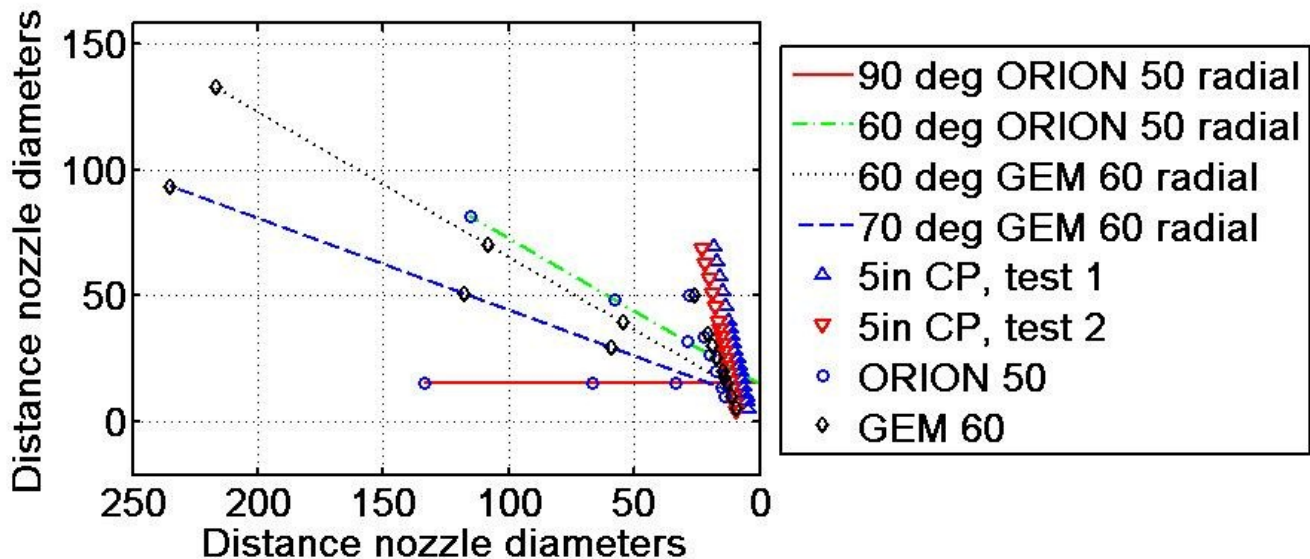
Figure 2.8 The combined layout of all of the microphones in the far field, having been normalized by nozzle diameter.

2.2 Method of extracting useable noise data

Just because a recording of rocket noise exists does not mean that it is ready to analyze in its entirety. Certain things must be done to take the raw recording and prep it for analysis.

2.2.1 Differences between probes

One of the first major factors is the way the different probes record. All of the microphones used in these tests were constructed by G.R.A.S.. Many of these probes and microphones are calibrated so that a positive increase in pressure corresponds to a positive increase in voltage. This includes the single microphones and those in the external frame tetrahedral probes. The only exception to this is a tetrahedral probe made by G.R.A.S. that is set inside of a sphere. This probe was designed so that a positive change in pressure would result in a negative change in voltage, leading to a flipped waveform. If using the original recordings please take note of this and flip them back to the proper orientation. The way one of these recordings from a spherical probe can be identified is by looking

at the noise distribution during the rocket firing. If the scale on the y-axis is more negative than positive than it is from a spherical probe and needs to be inverted. However, to avoid this problem there now exist cleaned up versions of these firings in a '.mat' format, which can be of great use to future analysis.

Another problem that was encountered with the two different probe styles is scattering. Due to the structure this caused scattering and interference at various high frequencies. The external frame tetrahedral had significant scattering off the nylon blocks that hold the microphone. The spherical probe suffers from the effects of spherical scattering. There was one other type of probe, the upright tetrahedral, which has had no noticeable scattering effects to which I am aware. However the preferred measurement tool in all these statistics is the single microphone.

This scattering had a tendency to increase or decrease the skewness and the kurtosis from its actual physical value (decrease it in the case of the external frame, increase it in the case of spherical). This can be especially seen in the 5in CP tests since it was a much higher pitch rocket and used both external frame and spherical probes. There really is no way to correct for it, but it is something to be aware of as the data is analyzed.

2.2.2 Removal of transient elements

Another thing that needs to be done to the recording in order to have a clean analysis is to remove all portions outside the significant thrust period. This was done to make the statistics as constant as possible without any fluctuation in power output.

However, removing the ramping up and ramping down portions was not easy. Most of this is done by eye and is not easily duplicated. The random nature of noise makes it difficult to work with. One solution that was purposed was to split the data into small segments and take the standard deviation. and once the standard deviation was above 80% of the the maximum standard deviation that that data segment would be used. There were several problems with this, especially since the

recordings sometimes lasted for several minutes and this would take too long for the computers to calculate. Also if there were any kinds of capacitance problems, as outlined in the next section, then the program would miss the real firing times. Up to this point the best I have been able to do is to personaly inspect each recording and guess. This process involves looking for the first time the overall amplitude reaches a flat value do find a start time, and then cutting it off at the end right before that flat value is left. A table of suggested start and end times for analysis is contained in Appendix A.

2.2.3 Microphone transient issues

Lastly, there was a problem that I encountered in a few of these recordings. As the noise was recorded I noticed a sudden and gigantic rise in pressure in some of the more distant microphones. It would be so large as to be obviously unphysical. The signal would continue to record at this higher level, but its mean instead of being at zero would fall off as $1/t$. This was the result of a capacitive discharge in the microphone, caused by the cable having too much resistance for the power supply to amply supply the microphone with current during a shock. [12] This destroyed the remainder of the recording since I and the rest of the BYU Acoustics Group do not know if the data can be trusted after the device has undergone such a shock. When such recordings were found I tried to work around the capacitive discharge as much as possible, throwing away any portions affected. Any recordings so affected will be noted in Appendix A.

2.3 Statistical methods

There are a couple of statistical methods unique to this study that must be addressed here. The first is the spatial evolution of the statistics and especially the PDF. The second is a brief discussion on the importance of looking at these statistics as they evolve in time, which is something BYU

Acoustics Research Group hopes to accomplish in the near future.

2.3.1 Spatial evolution of the statistics

In order to display the evolution of the statistics in space I have decided to show line graphs of the near field for skewness and kurtosis in terms of distance downstream in nozzle diameters. For the far field I have decided to do the same for the skewness and the kurtosis, but in stead of distance being given distance downstream, the distance be given in terms of distance along the radials in nozzle diameters.

The PDF's turned out to be slightly difficult to convey how they evolved in space as this was the first time this had ever been done. I decided to depict them as a three dimensional surface, with the x-axis being standard deviations, the y-axis representing distance ether downstream or along the radial in nozzle diameters (depending on if it was a near field or far field measurement), and the z-axis representing the value of the PDF at that point.

In Fig. 2.9 one of these PDF surfaces are shown. It is plotted on a log scale on the z-axis to provide for the clearest view of the tails in positive and negative x directions, since this is what most significantly impacts the statistical moments in this study. Note however that is viewed from the top. This allows easier observation of the tail's evolution along the y direction. Note how it has very square edges, this is an artifact from having only a few recording points instead of a constant array of microphones (which unfortunately would not be feasible). I would assume in actuality that the transition is much more smooth.

2.3.2 The time evolution of statistics

As stated previously, these measurements were taken under the presumption that the noise had constant statistics over the course of the entire recording. The entire wave, except for the parts already removed as explained, would be analyzed as a whole, with the hope that the statistics were
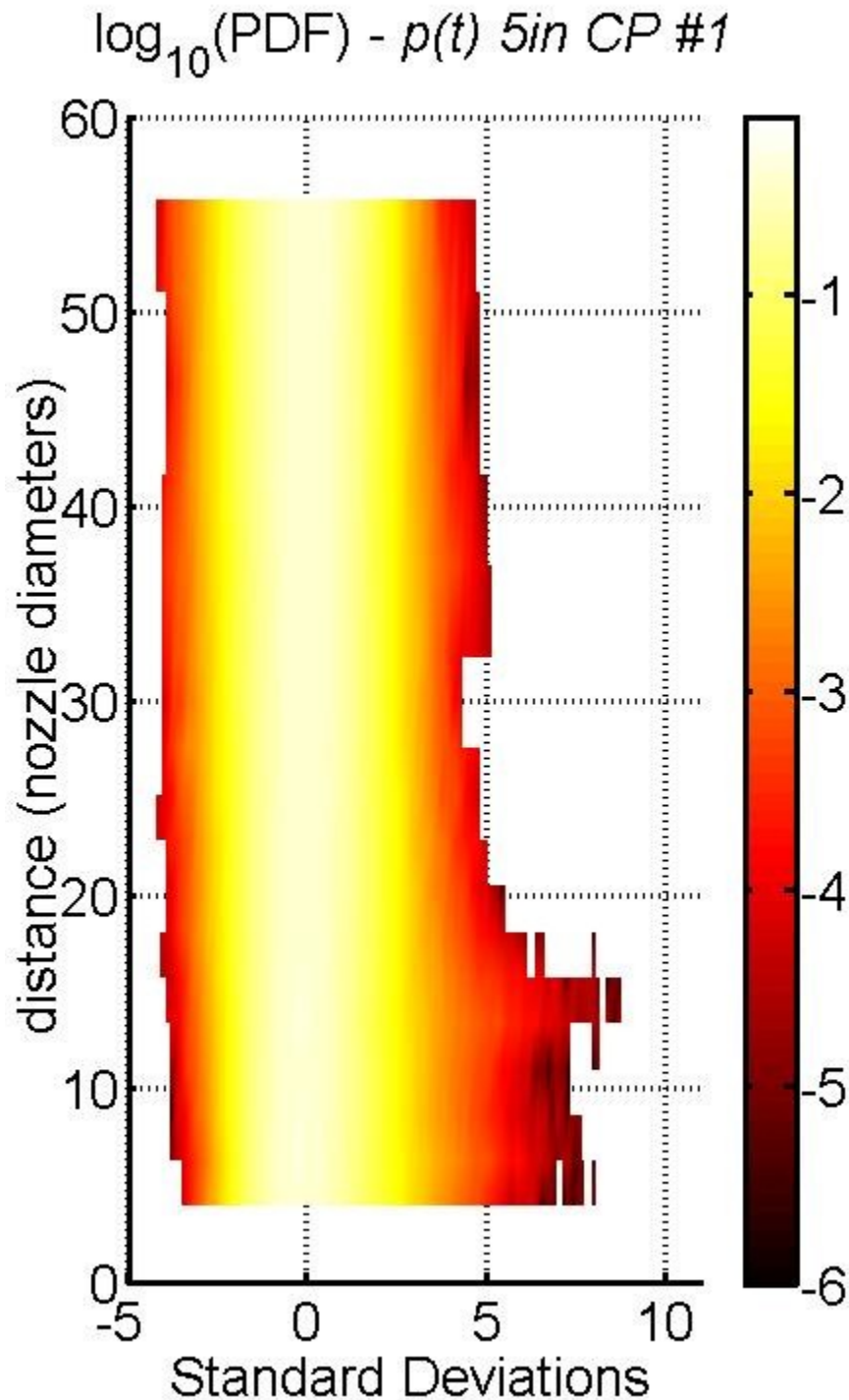
Figure 2.9 This is the method I will use to show the PDF evolving in space. The horizontal axis corresponds to the x axis in a normal PDF. The z axis (out of the page) corresponds with the y axis of a regular PDF. The vertical axis is the distance along a particular line of microphones. This "top-down" view allows a clear view the behavior of the tails in each PDF as it evolves in space.

for the most part stationary. This assumption in truth is not valid due to the variations in power output by the rocket. I anticipate that this time variation in the statistics will be especially evident in the ORION 50 recordings and statistics as the nozzle was gimballed or moved over the course of the test. Dr. Gee has hopes to test this in the near future by subdividing the wave into small millisecond chunks that have enough data points to be statistically stable, and then plot the statistics at given points in time.

Chapter 3

Results and Conclusions

3.1 Results

3.1.1 Probability density function comparisons

After executing the data analysis as explained earlier the following PDF's were obtained: Figs. 3.1 and 3.2. The first set, Fig. 3.1, is of the shear layer, each one from left to right is closer to the plume. Fig. 3.2 shows the radial lines in progression from perpendicular to the plume on the left , progressing to the closest to the shear layer on the right. One of the first things that jump out is that in Fig. 3.1, the PDF's all have the same general shape. They are initially very positively skewed with large positive outliers. These positive outliers would be shocks or large peaks relative to the noise that would eventually transform into shocks. The noise however appears to become more Gaussian over time. This could be in part due to the randomizing effects of thermal motion. Another contributor to this loss of skewness is nonlinear attenuation of shocks, which reduces the amplitude of the shocks relative to the noise, thus removing the large positive outliers in the PDF.

Even with this decay though, note how the general values stay roughly the same. The colors at -3 standard deviations and 5 standard deviations show very little difference in the near field,

though in the far field some visible narrowing of the PDF has occurred. A possible explanation for the difference between the near and far field is that since the far field have a much greater distance to cover, the randomizing effects of particle motion have had more time to affect the wave. Now, since each of these graphs are on the same scaling it can be seen that these values not only evolve at similar rates but that they are similarly valued. This remarkable similarity between these PDF's show that rocket PDF's truly can be collapsed upon each other, something which will be discussed latter.

Another great similarity can be seen when one plots the PDF's in the usual way at the maximum sound location of each rocket. When this is done, as seen in Fig. 3.3, the difference between each PDF is quite small, and the distributions look nearly identical. This fact seems to suggest that there could be another way to compare rockets biased on the location of their maximum OASPL, which could be the work of some future paper.

The PDF's of the time derivative are given in Figs. 3.4 and 3.5, and also have the same layout and orientation as the ones shown before. When they are compared to each other I find that the PDF's are all radically different, with the outliers becoming more prominent downstream in the more powerful rockets. One thing of note is that the outliers are almost nonexistent in the smaller 5in CP. This is very much in harmony with our understanding of noise and shock formation since the 5in CP was a less powerful rocket. Something to remember as these graphs are analyzed is that the positive outliers here are not a mixture of high pressures and shocks like in the earlier PDF's, but that they are all shocks. The reason why the positive outliers become more prominent downstream as opposed to the previous PDF's is because the shocks are subject to nonlinear attenuation. This makes whatever shocks that were present deteriorate in amplitude until they cannot be differentiated from the rest of the noise by its amplitude alone and the PDF becomes more Gaussian. But in the derivative, the near infinite slope is still visible regardless of amplitude. Farther downstream, where there would be a greater distance from the center axis of the plume (the assumed source lo-
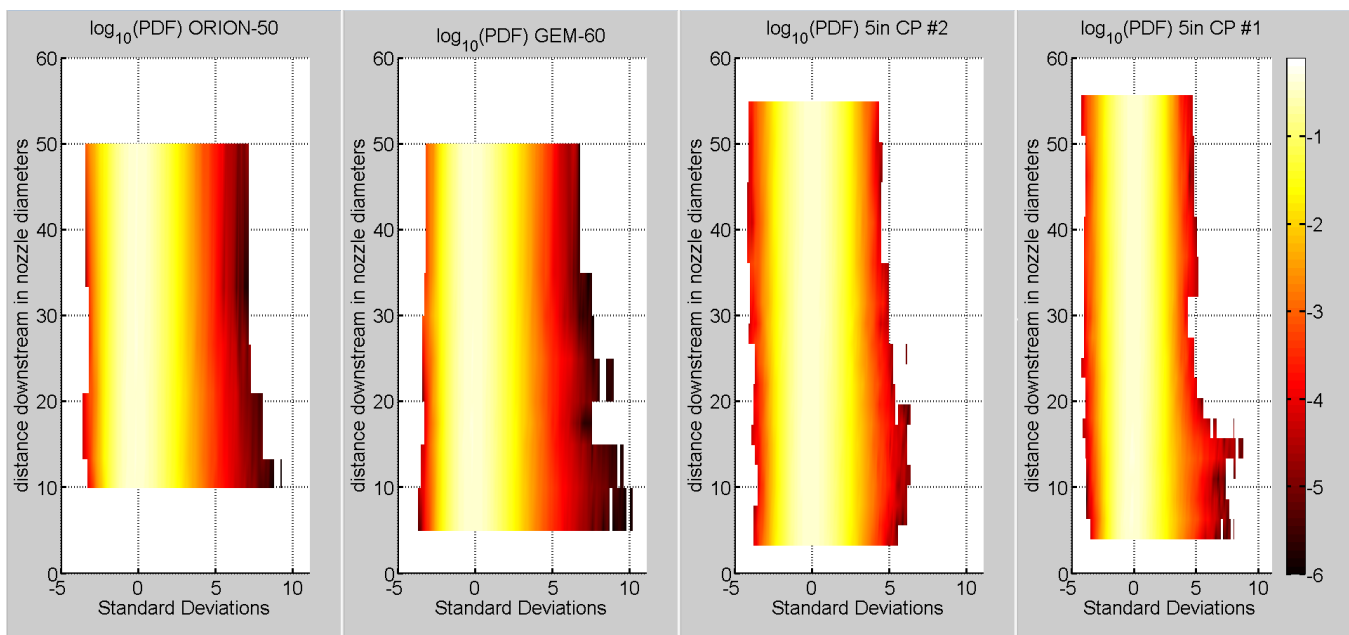
Figure 3.1 A comparison of the PDF's of the different shear layers. Notice that they all have the same basic evolution from positively skewed to becoming more Gaussian with less and less positive outliers. Also notice that they all have approximately the same values at positive 5 and negative 3
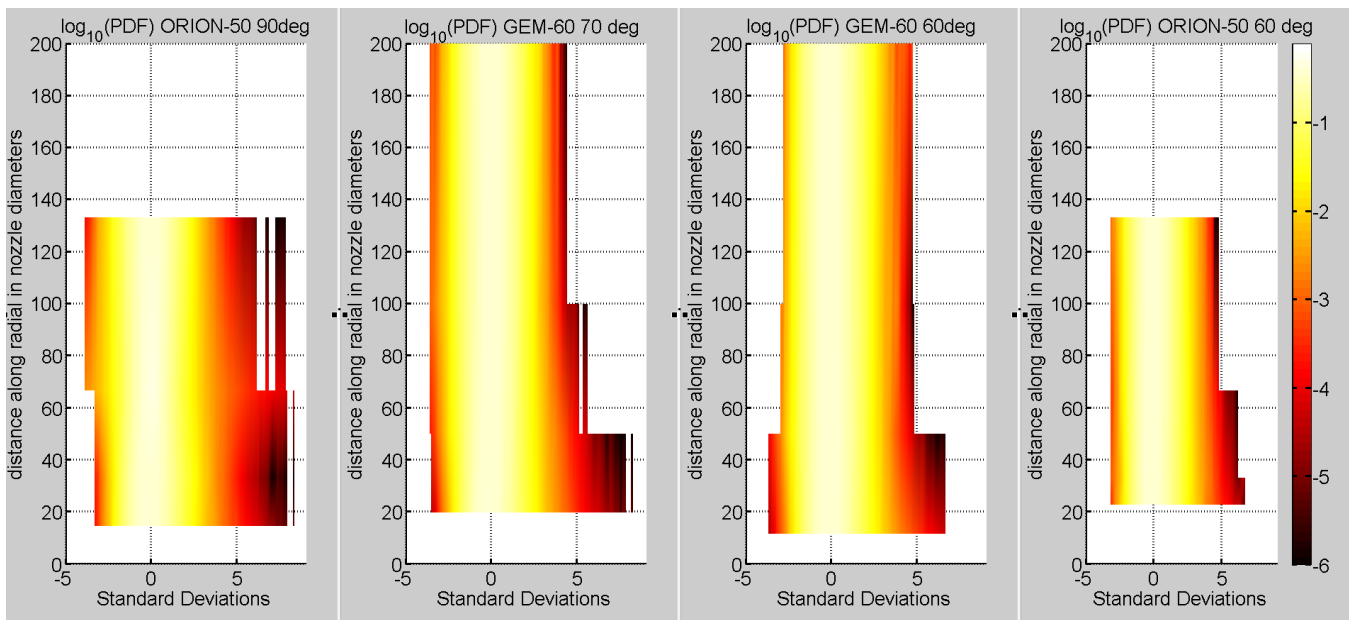
Figure 3.2 A comparison of the PDF's along the radials. Notice that they hold approximately the same values at -2 and 4, but that there is some shift by the end to a more symmetrical Gaussian. Overall it is very similar to the evolution in the near field, just more advanced.
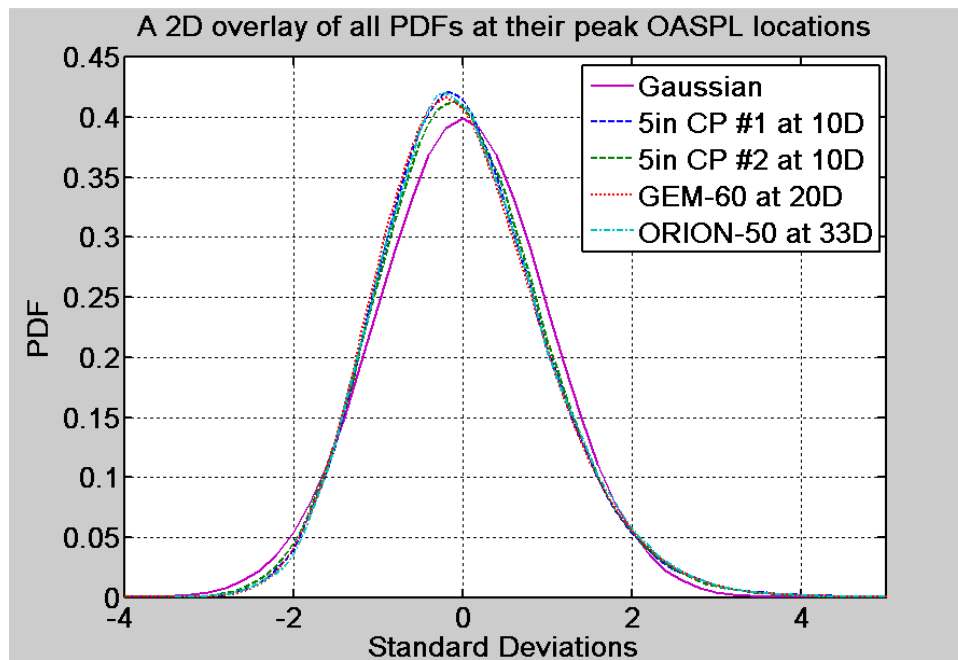
Figure 3.3 A two-dimensional PDF comparison of all rockets in this study at their maximum OASPL, which locations are given in the legend. The most amazing thing to note with this graph is that when the comparison is done at the maximum sound level rather than distance that the PDF's collapse on eachother with very little difference, suggesting yet another way to compare rockets.
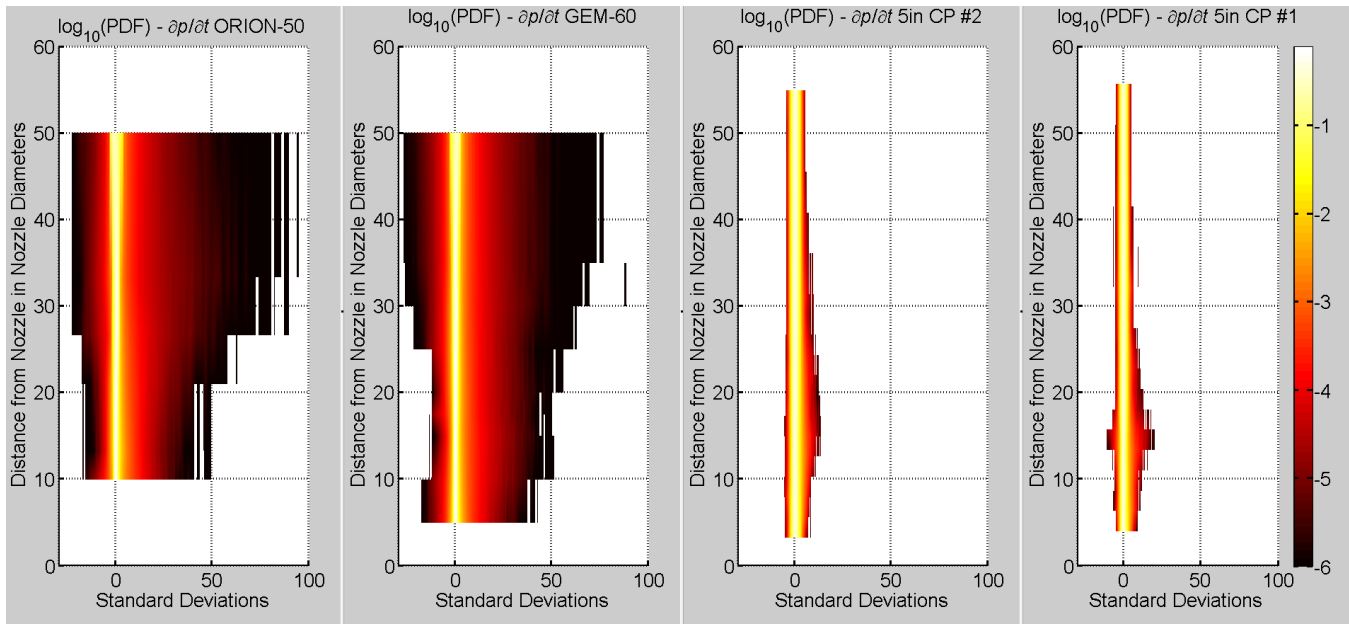
Figure 3.4 A comparison of the time derivative PDF's of the different shear layers. Notice that they all have radically differing values. These values are all dependent on the content of shocks.

cation), more shocks can form as lower amplitude peeks have finally caught up with the troughs in front of them. Thus the PDF of the derivative, and the amount that it is positively skewed, shows the density of shocks in the waveform. Thus it appears that the 5in CP does not have enough power to generate shocks, but that the other two do, and that the farther away something is from the plume the more shocks it will undergo. However, with nonlinear attenuation there is a counterpoint that the farther away something is from the plume, the weaker the shocks will be.

Now there is one strange quality that has not yet been fully explained here that has to do with the far field. The 90° radial PDF has a very different shape, one that Does not fit the normal pattern. It is smaller, which denotes that there is a directionality to shocks. This shape almost seems to indicate that the noise here is not as nonlinear, or at least it is not "shocked up."
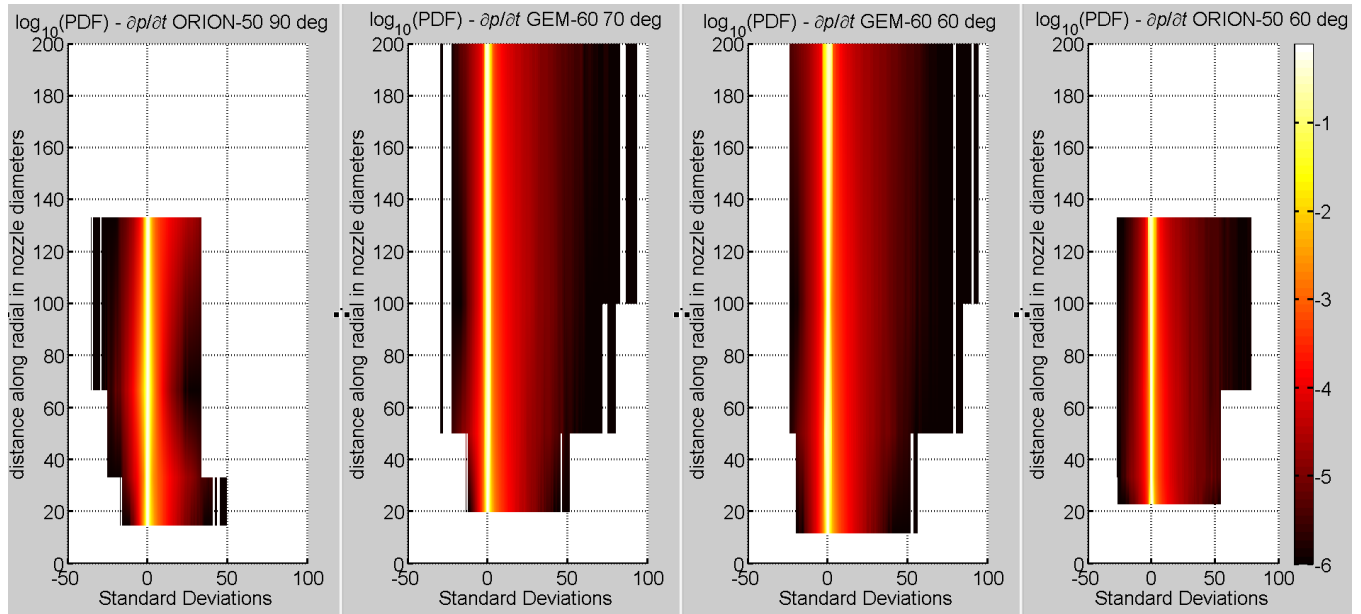
Figure 3.5 A comparison of the time derivative PDF's along the radials. Note how all except the 90° radial follow the same basic trends. This last radial does not follow the same pattern as the others and it appears that it does not have as much shock content as the others, confirming the theory that shocks are directional.

3.1.2 Skewness and kurtosis

Figs. 3.6, 3.7, 3.8, and 3.9 show the evolution of the skewness and kurtosis in space for both the data and the time derivative between the different rockets. Note that there really is no notable difference between the evolution of the skewness and the kurtosis. Since the skewness is the most traditionally used it will probably remain the standard measure in this field. The same patterns as discussed in the previous section of drops in skewness in the data farther downstream, and massive jumps in the statistics of the time derivative are seen here. Note that in these figures that the lines for the 5in CP are almost impossible to see in the derivative. This reflects that there is probably little to no shock content in this rocket far downstream from it.

There has been some work done on the subject of shock formation distance in noise [4], even though there really is no uniform shock formation distance as discussed in section 1.3. Instead of
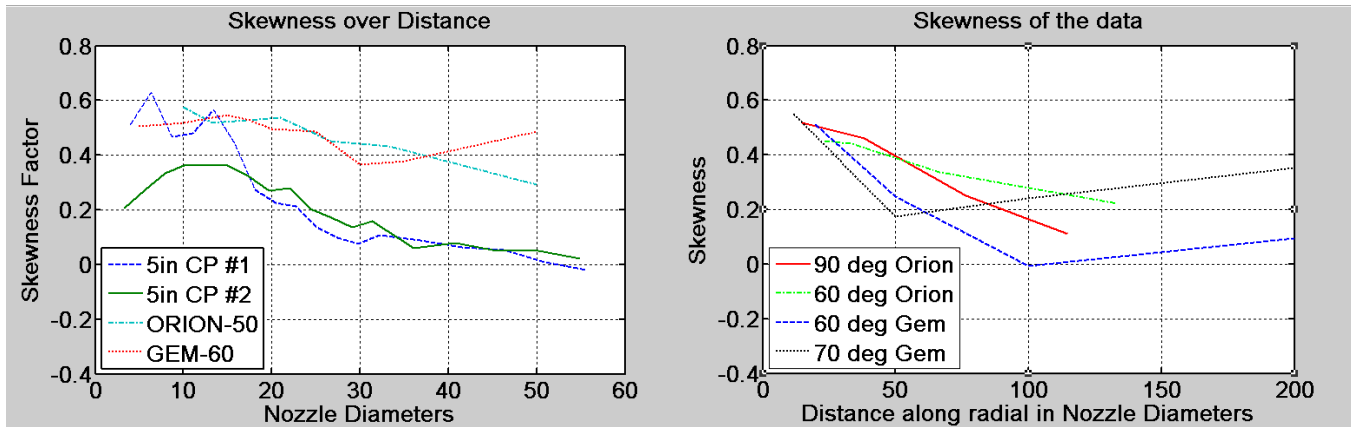
Figure 3.6 The first figure shows the skewness evolving in space for the shear layers, the second shows the evolution of the skewness along the radials.
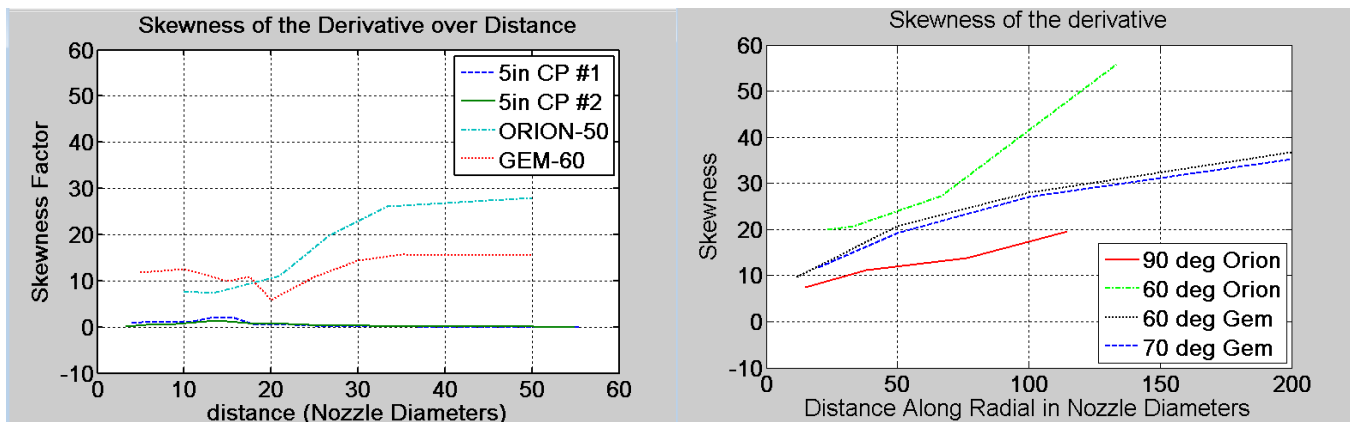
Figure 3.7 The first figure shows the skewness of the time derivative evolving in space for the shear layers, the second shows the evolution of the time derivative skewness along the radials.
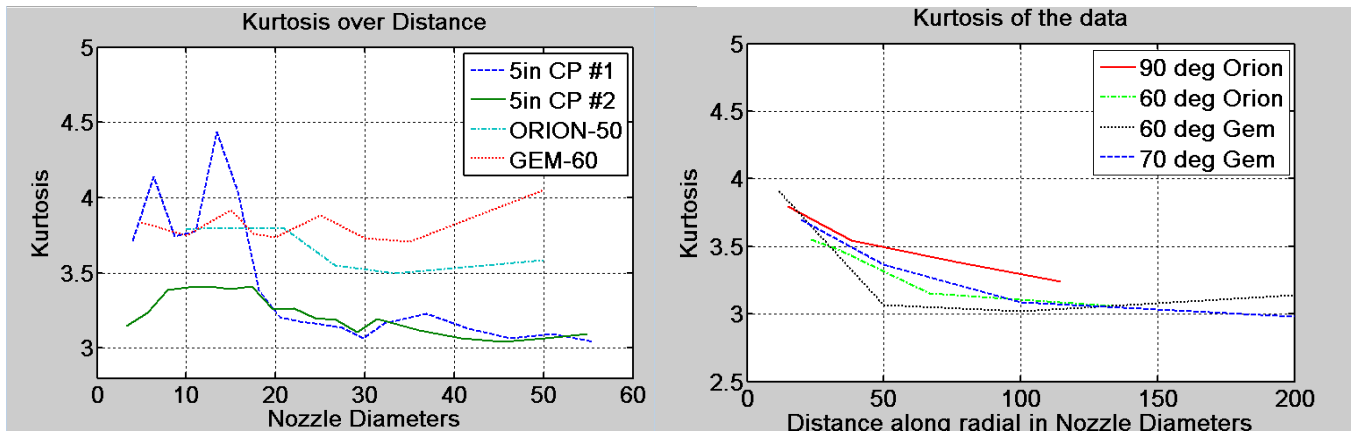
Figure 3.8 The first figure shows the kurtosis evolving in space for the shear layers, the second shows the evolution of the kurtosis along the radials.
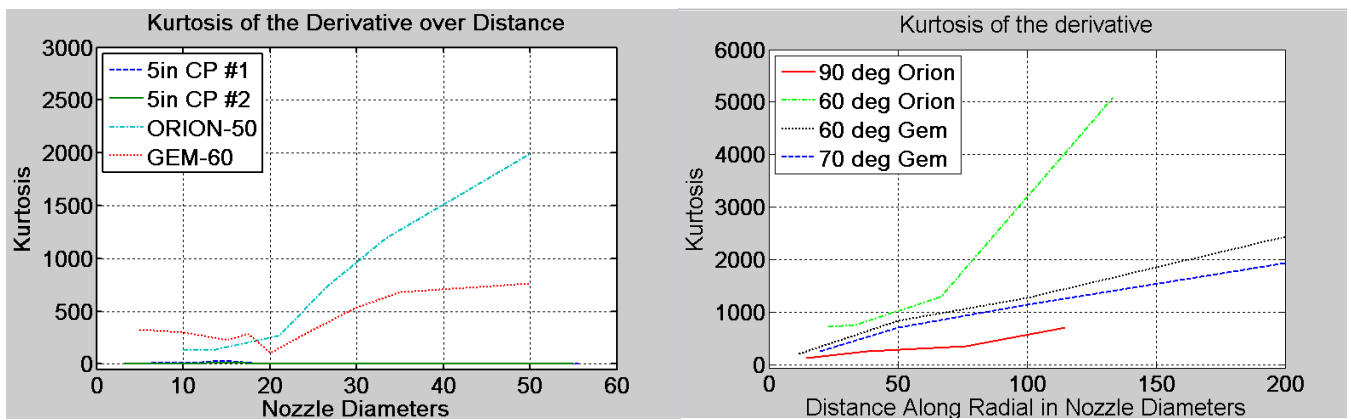
Figure 3.9 The first figure shows the kurtosis of the time derivative evolving in space for the shear layers, the second shows the evolution of the time derivative kurtosis along the radials.

asking for a concrete formation distance it is possible to instead ask if there is a range of shock formation, or ask when shocks first form within the noise. Though at this point I are not entirely sure of where that would be, it seems that this distance is evident in the skewness and kurtosis of the derivative as it goes from a relatively flat value, and then jumps significantly. The shock formation distance in the GEM 60 and ORION 50 rockets is approximately 25 nozzle diameters downstream. The fact that the GEM 60 and ORION 50 statistics are in such harmony over a scaled distance implies that this may be a common saleable characteristic of rocket motors.

3.2 Analysis

These results are very important because they show that for these three rockets that the statistics can be collapsed to the same shape for the PDF of the original recording. This implies that something physical about rocket noise will always generate this kind of distribution. It is also exciting because if this same process is carried out for the derivative crucial differences can be easily uncovered. However, this process has only been applied to these three rockets. Could it be a phenomenon that is unique to the rockets I have chosen?

In an effort to put this question to rest the PDF's I have generated were compared to PDF's from other studies in rocket and jet noise. These comparisons are found in Fig. 3.10. As these PDF's are compared the same trends that I found before are evident. They have the same basic shape, are positively skewed, and approach zero at about -3 and 5 standard deviations. In every instance this holds true. Thus it is confirmed that there is something about the mechanism of rocket and jet propulsion that creates this kind of pressure distribution.

What about the PDFŠs of the derivative, how do they compare to previous studies? The problem is is that this is a relatively new method of describing the content of shocks within the noise, and thus only a few graphs exist. However, when the few available are compared to the ones in this
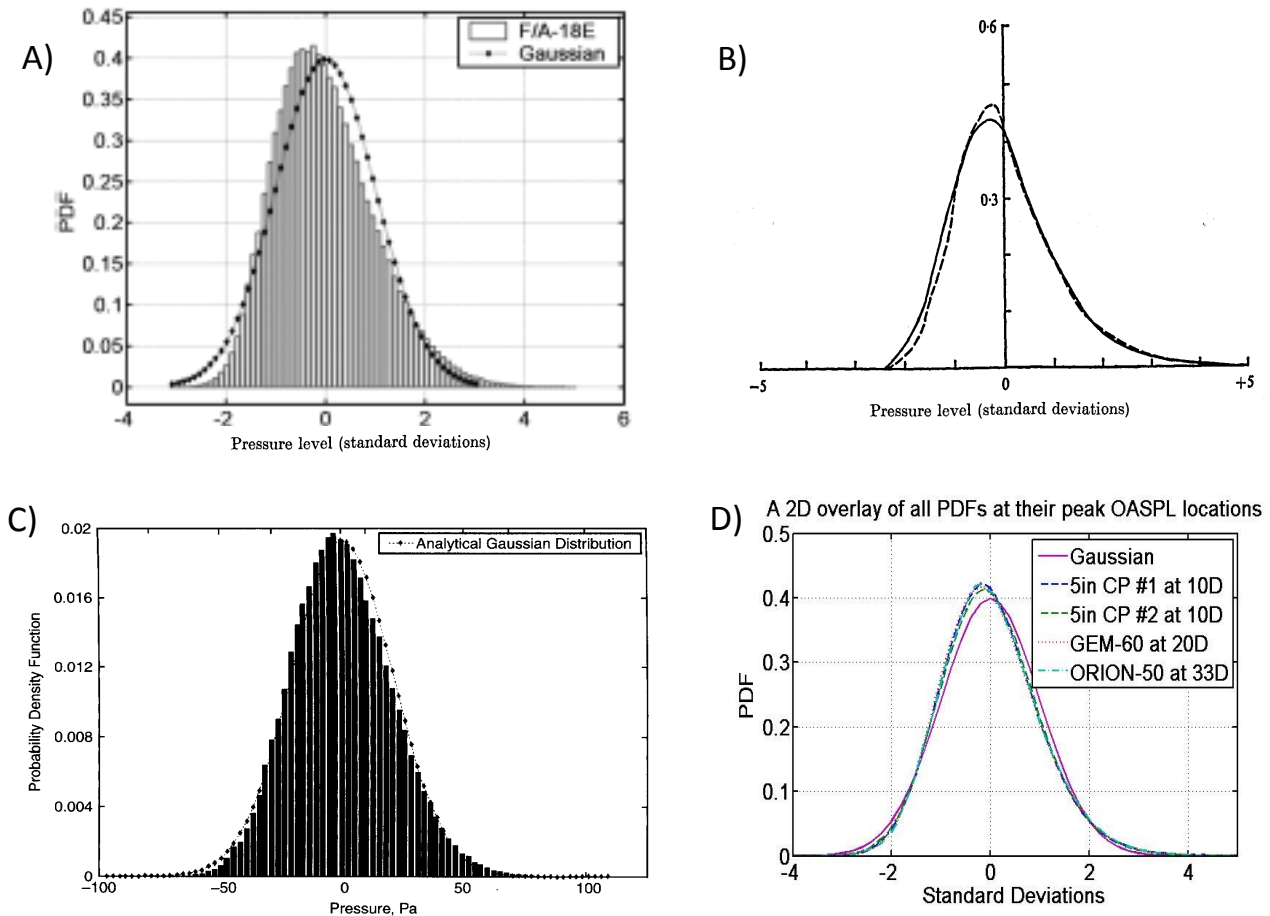
Figure 3.10 A comparison of the PDF's shown in this study and those taken before by others. Figure A) A PDF of an F/A-18E at afterburner compared to a Gaussian distribution [5]. Figure B) A PDF of the Olympus 592 engine and a 1:10 scale model [6]. Figure C) A PDF of a supersonic jet [9]. Note that even though it is not normalized on its x axis I have effectively done so myself by making the Gaussian comparison the same size and shape as the one in figure A. Figure D) A comparison of the four shear layer PDF's at a similar distance downstream with a Gaussian comparison. Notice that the PDF's all have the same shape, and all decay to basically zero at -3 and 5.

study the tendency still holds that each are radically different, as can be seen in Fig. 3.11. This has much to do with the amplitude of the rocket or jet. If the rocket does not have sufficient power in order to achieve the sound amplitude necessary for shocks to form, then a PDF similar to the 5in CP could be expected. On the other hand, if the rocket does have sufficient power to form shocks then there will be a great amount of skewness and positive outliers in the PDF of the derivative.

3.3 Conclusions and directions for further work

From this study I have reached the following conclusions: First that PDF's of solid rocket motors and jet afterburners have the same basic shape regardless of size. This is an important property which may in the future help us better understand the physical nature of what is happening in this highly nonlinear, turbulent flow. Second, that all solid state rocket motors have similar evolution in space for the PDF when distance is scaled by nozzle diameter, regardless of rocket size. Once again, this is an important property to understanding how the sound from a rocket or jet propagates. Third, that skewness and kurtosis are basically equal in determining the presence of shocks. Fourth and lastly, that the PDF of the derivative from any rocket or jet will differ depending on the amplitude of the sound and the presence of shocks.

There are three major areas where this work could proceed. The first is to widen its scope to larger rockets to see if the trends noted here continue. Noise data from the Space Shuttle RSRM would be incredibly useful in this regard. This is a 12.5ft (3.81m) diameter rocket, and would put an upper limit on the solid rocket motor study. If the same trends continue it could be assumed that all solid rocket motors with an exit diameter in between this study and the RSRM behave the same.

The second direction is to extend this test from the 5in. to 3ft. nozzle range, and to see where the limit lies between the absence and presence of shocks. It is probable that there is not a strong
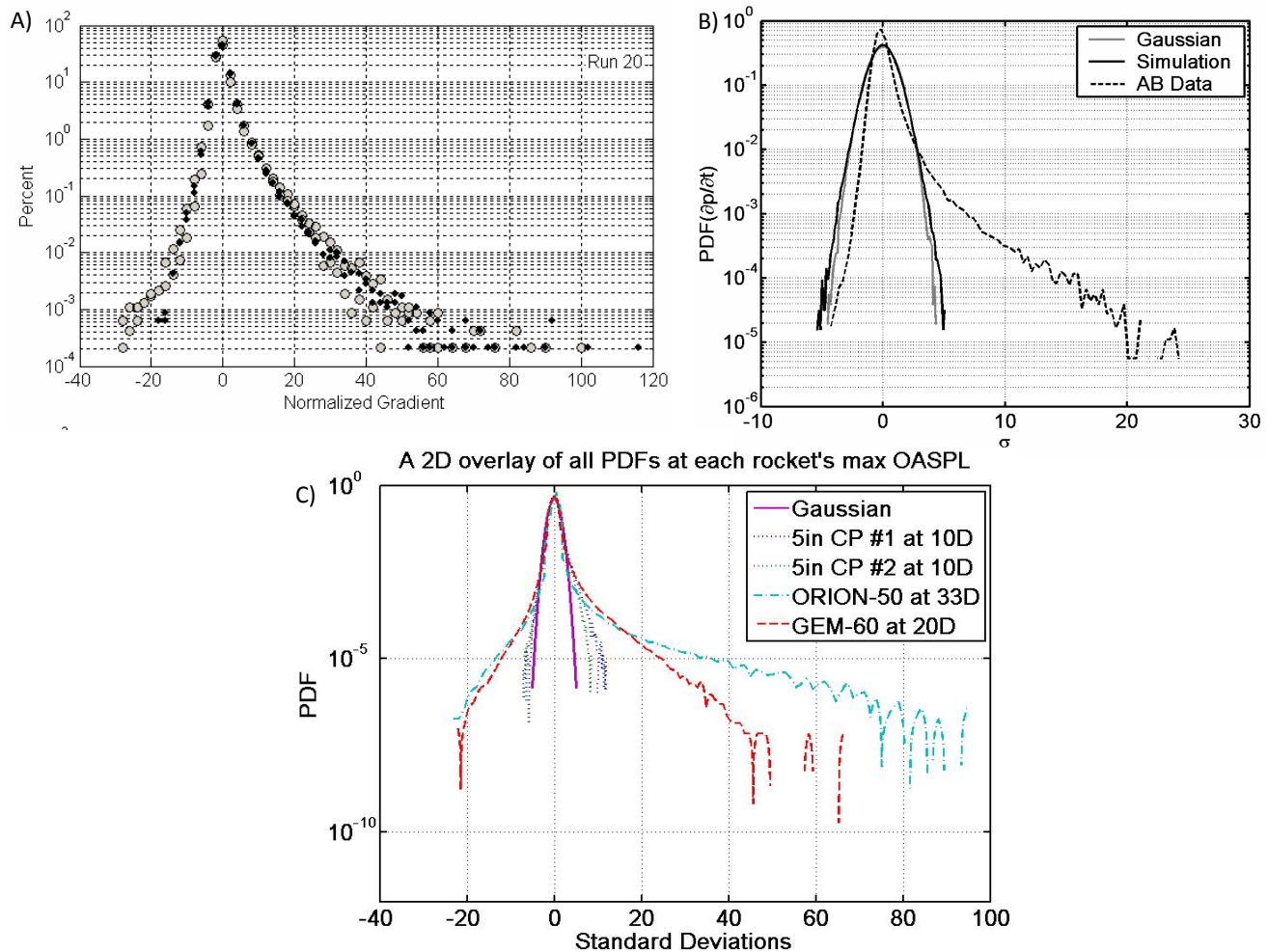
Figure 3.11 Figure A) A time derivative PDF done of an aircraft afterburner flyover [8]. It is not clear from her paper if the x-axis corresponds to the other graphs shown here. It is still included in its published form to show its basic shape. Figure B) A time derivative PDF of some simulated afterburner data without shocks (but yet statistically the same) and actual F-18E Afterburner data [5]. Notice how without shocks the derivative PDF is essentially Gaussian. Figure C) A comparison of the PDF's of the time derivative of all the rockets in this at about 25D downstream. Note how different they all are. The rockets that were powerful enough to create shocks all have significant skewness, while the 5in CP is almost Gaussian in comparison, showing little to no shocks in the data. This is consistent with Figure B).

cutoff point as even the 5in CP looked like it could have had some minor shocks forming around 15 nozzle diameters on its closest shear layer but did not have the power to sustain them. It would be interesting to see where and under what conditions shocks are most likely to be formed.

Third, there is the question on how much power is required. Note that the 5in CP had much less fuel to burn than the others, and hence the behavior could be more an effect of the amount of propellant burning at a given time rather than nozzle diameter. Studies of smaller yet stronger rockets are needed to further understand this phenomenon, as well as larger yet weaker rockets. Noting this with the other notes above it is seen that this is merely a small string of data in a multidimensional volume of possibilities. It is a marked improvement over the scattered, unconnected data points that were had before this study, but there is still much to be explored.

Lastly, the issue of time evolution in the statistics has yet to be addressed. As mentioned previously, each of these statistical results was done under the false assumption that these noise sources are statistically constant in time. I know this assumption is false because the thrust profile for each of these rockets is not constant in time, and thus there will be some differences over time in the basic properties of the noise. Could it be that there is some underlying pattern here between all rockets that has been glossed over by making this assumption? Further research into this could be highly rewarding.

Appendix A

Rocket information

In this appendix I will go over the more rudimentary information about the rockets. Each rocket will be gone over in detail. Below is Fig. A.2 showing the standard deviation pressure for each rocket as it evolves in space. As discussed at the end of section 2.1.3, there is a discrepancy between what I calculated and the results from a previous paper by Gee et al. [11] This was once thought to be a calibration error, but after receiving recalibrated data I found that this error did not go away and I am at a loss to reconcile them. If there is a question on which is more accurate, go with the one made by Gee et al.

A.1   5 inch CP

The data for this rocket were obtained from the recordings described below. There are many more recordings there than are dealt with here. ID 1 is a test recording run with no rockets. Channels 16-18 are the three stationary microphones, whose positions were not recorded, unfortunately.

The first table here describes the moving probe apparatus. Probe is the probe type, weather spherical (NASA) or external frame (Ext.). Channels explains which channels belonged to each probe with the channel used in this study in parentheses. X mod and Y mod states how many
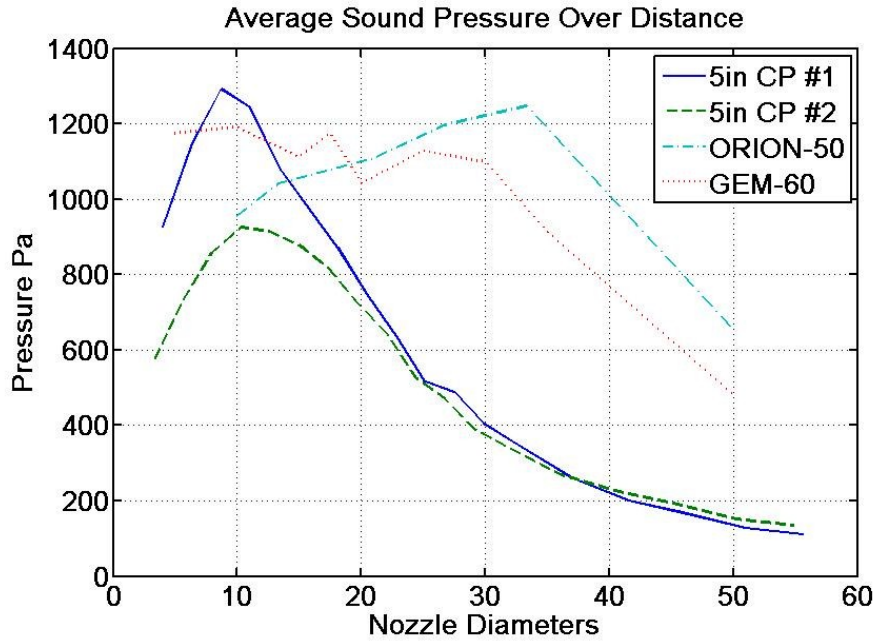
Figure A.1 The RMS pressure of each of the rockets in space. Note how the pressure is much lower on the 5 in CP even though its microphones are so much closer than the other rocket's microphones. This suggests the lack of power of the 5 in CP compared to the other two rockets.
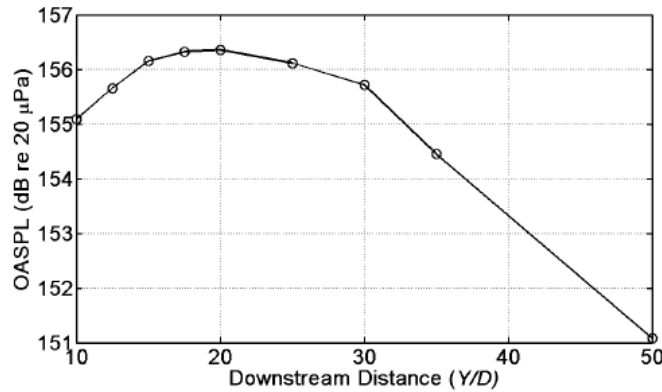
Figure 13. Near-field overall sound pressure level as a function of distance downstream during the 2-19-09 GEM-60 firing at ATK.

Figure A.2 As can be seen by comparing this to the previous figure, there are some significant discrepancies between what I have found for the sound pressure for the GEM-60 and what was found before by Gee et al [11]. If there is a question on which one to use, use this one because I believe it is more accurate.

inches or nozzle diameters (ND) need to be added or subtracted from the position given for the ID in the second table.

The second table states the recording ID number, the position number, and the location of probe 1 in inches and nozzle diameters. It also states the following times in the recording in seconds: when the rocket was first ignited (ig. time), when the noise becomes stable enough to start analyzing (st. time), when the recording ceases to be stable and analysis ends (end time), and when the rocket dies out (die time).

ID 9 Channel 8 has a capacitive discharge at 7.1 seconds (thankfully after the rocket was finished). The usual start and end times for that ID should remove it. There are other recordings that have the transient elements already removed.

Probe	Channels	X mod.(in)	Y mod.(in)	X mod.(ND)	Y mod.(ND)	Notes
NASA	0-3 (0)	0	0	0	0	invert wave
Ext.	4-7 (4)	-10.2	20.25	-2.04	4.05	invert wave
Ext.	8-11 (8)	-16.29	-7.65	-3.26	-1.53	
Ext.	12-15 (12)	-26.49	12.60	-5.30	2.52	

ID	Pos.	x(in)	y(in)	x(ND)	y(ND)	ig. time	st. time	end time	die time
2	1	-18	20	-3.6	4	5.4	5.5	8.25	8.35
3	1	-18	20	-3.6	4	2.72	2.8	5.5	5.65
4	2	-27.98	66.95	-5.60	13.39	1.95	2.00	4.7	4.9
5	2	-27.98	66.95	-5.60	13.39	3.03	3.09	5.7	5.9
6	3	-37.96	113.90	-7.59	22.78	2.02	2.2	4.8	5.0
7	3	-37.96	113.90	-7.59	22.78	2.96	3.05	5.7	5.9
8	4	-47.94	160.85	-9.59	32.17	2.45	2.6	5.2	5.5
9	4	-47.94	160.85	-9.59	32.17	2.87	2.95	5.6	5.8
10	5	-57.92	207.8	-11.58	41.56	2.73	2.85	5.4	5.7
11	5	-57.92	207.8	-11.58	41.56	2.29	2.5	5.00	5.3
12	6	-67.90	254.76	-13.58	50.95	2.2	2.3	4.9	5.2
13	6	-67.90	254.76	-13.58	50.59	1.84	2.00	4.6	4.8
14	1.25	-20.49	31.74	-4.10	6.35	2.23	2.3	4.95	5.1
15	1.25	-20.49	31.74	-4.10	6.35	2.28	2.35	5.05	5.2
16	2.25	-30.47	78.69	-6.09	15.74	2.7	2.8	5.5	5.7
17	2.25	-30.47	78.69	-6.09	15.74	2.5	2.55	5.2	5.4
18	3.25	-40.45	125.64	-8.09	25.13	1.98	2.1	4.8	4.95
19	3.25	-40.45	125.64	-8.09	25.13	1.98	2.1	4.75	5.00

A.2 Orion 50

The Orion 50 recordings were all taken with one firing, thus there is only one ID number, ID 1. I analyzed 20 seconds of data, beginning at 41 minutes 56 seconds. I ended at 42 minutes 16 seconds. By doing this I was able to avoid any corrupted portions from capacitance discharges. The table below outlines the positions for each recording, the type of probes used, and notes on

each recording.

With respect to the table below, the P.A.T. probe is a parallel axis tetrahedron, since it was not used in the test I have not gone into depth about it. Note A: This probe lost its upright microphone channel 50 seconds into the test, thus it is discarded. Note B: since there are so many probes in the same location, these too are discarded in favor of probe 3c.

Position	Probe	Channels	x(ft)	y(ft)	x(ND)	y(ND)	Notes
1	1/8" mic	28 (28)	40.91	30	13.63	10	
2	NASA	0-3 (0)	44.55	40	14.85	13.33	invert wave
3a	NASA	4-7 (none)	51.83	60	17.27	20	note A
3b	Ext.	16-19 (none)	52.43	60.31	17.47	20.10	note B
3c	Ext.	20-23 (20)	53.18	62.81	17.72	20.93	
3d	P.A.T.	24-27 (none)	52.70	62.66	17.56	20.88	note B
4	1/8" mic	29 (29)	59.11	80	19.70	26.66	
5	NASA	8-11 (8)	66.39	100	21.13	33.33	invert wave
6	1/8" mic	30 (30)	84.59	150	28.19	50	
7	1/8" mic	31 (31)	100	45	33.33	15	
8	2D	38-40 (38)	200	45	66.66	15	
9	1/8" mic	41 (41)	400	45	133.33	15	
10	NASA	12-15 (12)	96.59	70.88	32.19	23.62	invert wave
11	1/8" mic	32 (32)	86.60	95	28.86	31.66	
12	2D	42-44 (42)	173.2	145	57.73	48.33	
13	1/8" mic	45 (45)	346.41	245	115.46	81.66	
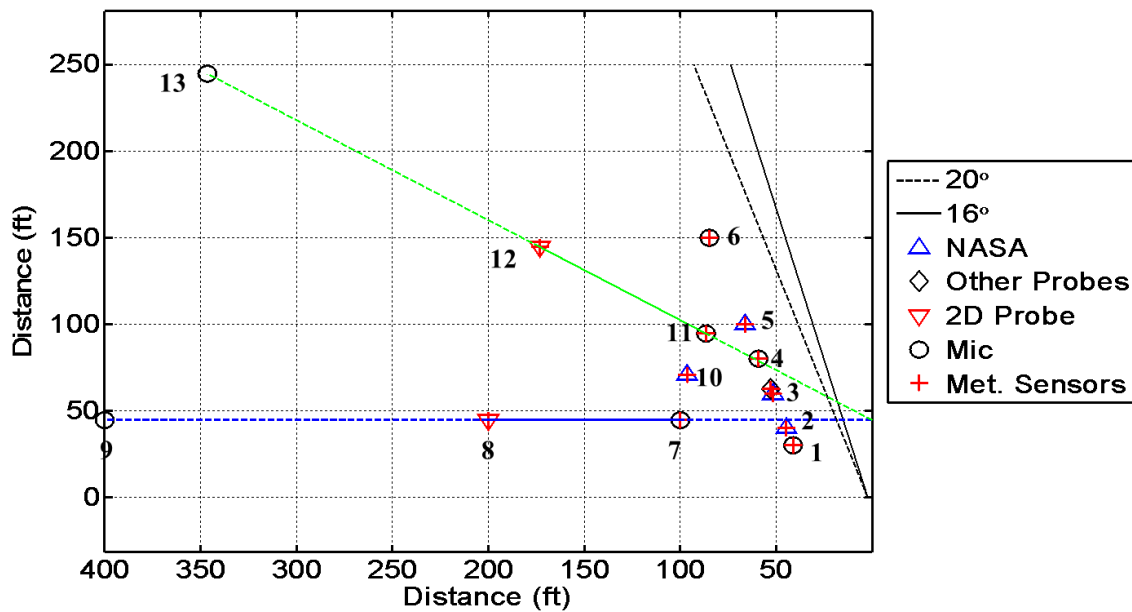
Figure A.3 The layout of the microphones for the Orion 50 test.

A.3   GEM 60

The GEM 60 recordings were all made with one firing. Analysis began 22 minutes and 20 seconds into the recording and ended at 22 minutes and 40 seconds. Separate data files have been created to reflect this as well as repair the calibration errors in some microphones. In this way I was able to invert the waves to their correct form and remove any transient elements, dead recording times, or corrupted recordings from capacitive discharge. If using the original recordings use the code I have outlined in the next appendix as well as this table. Note A: The cables for channels 33 and 36 were accidentally switched. The correct layout for all future reference is given in this table.
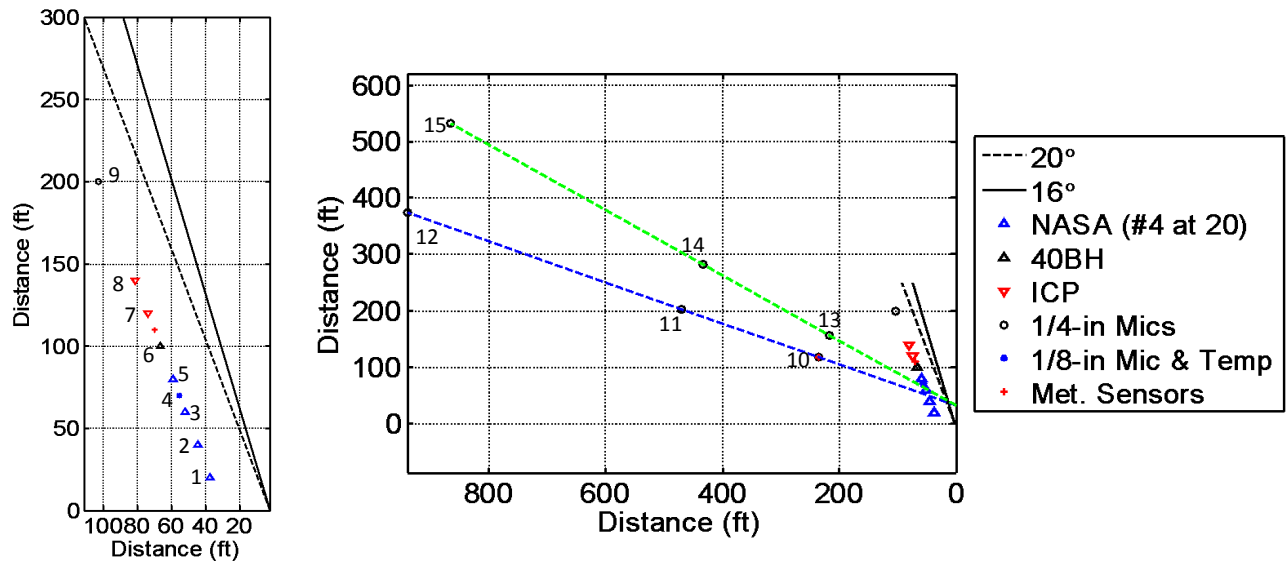
Figure A.4 The layout of the microphones for the GEM 60 test.

Position	Probe	Channels	x(ft)	y(ft)	x(ND)	y(ND)	Notes
1	NASA	12-15 (12)	37.3	20.0	9.32	5.00	invert wave
2	NASA	8-11 (11)	44.6	40.0	11.14	10.00	invert wave
3	NASA	4-7 (4)	51.8	60.0	12.96	15.00	invert wave
4	1/8" mic	28-30 (28)	55.5	70.0	13.87	17.50	invert wave
5	NASA	0-3 (0)	59.1	80	14.78	20	invert wave
6	Ext.	16-19 (16)	66.4	100.0	16.60	25	invert wave
7	Ext.	20-23 (20)	73.7	120.0	18.42	30.00	
8	Ext.	24-27 (24)	81.0	140.0	20.24	35.00	
9	1/4" mic	31 (31)	102.8	200.0	25.70	50	
10	1/4" mic	32 (32)	234.9	117.5	58.73	29.38	
11	1/4" mic	36 (36)	469.8	203.0	117.46	50.75	note A
12	1/4" mic	34 (34)	939.7	374.0	234.92	93.51	
13	1/4" mic	35 (35)	216.5	157.0	54.13	39.25	
14	1/4" mic	33 (33)	433.0	282.0	108.25	70.50	note A
14	1/4" mic	37 (37)	866.0	532.0	216.51	133.00	

Appendix B

MATLAB Code

The following is the code I used to accomplish this. It can be found under my file in the Kirchhoff Acoustics Storage Drive. (Z:\Students\Stuart Harper \The_ Mothercode_ 10_ 27_ 2011)

```
Editor - Z:\Students\Stuart Harper\Active Data analisis\ORION\The_Mothercode_10_27_2011.m*

File  Edit  Text  Go  Cell  Tools  Debug  Desktop  Window  Help

Stack: Base

 1        % Stuart Harper
 2
 3        % The Mothercode: This is to be a grand amalgamation of
 4        % Statistical_Analisis_7_1_2011, PDF_Averager, and PDF_overlaper_8_5_2011.
 5        % This will take an entire microphone's data from start to finish in one
 6        % fell swoop. This I feel will greatly speed up analisis and alow for the
 7        % future GEM and ORION analises to go much smoother.
 8
 9        % Flush the system
10 -      clear all;
11 -      close all;
12 -      clc;
13
14        % Set parameters for all line graphs
15 -      set(0,'DefaultFigurePosition',[-3 39 1280 916]);
16 -      set(0,'DefaultAxesLineWidth',2);
17 -      set(0,'DefaultLineLineWidth',2);
18 -      set(0,'DefaultAxesFontSize',20);
19
20        % Acsessing the Data
21 -      pathname='Z:\Dr Gee\Field Data\Orion50\';
22 -      testname='ID';  % Root test name from Data Recorder
23 -      ID=1;   %Test Run
24 -      CH=[29 32 42 45];   % Channel Number
25        % distance downstream or along radial for each chanel in Nozzle Diameters
26 -      Scale=[22.9,33.332,66.665,133.33];
27 -      fs=204800; % Sampling Frequency (Hz)
28 -      histbins=91; % Number of Histogram bins
29
30        % Test Function - Used to create the Standard Gausian function used for
31        % comparison purposes
32 -      Summer=-5:.2:5;
33 -      test=(1/(2*pi)^(1/2))*exp(-(Summer.^2)/2);
34


35        % Prefabricate the arrays to speed up the loop
36 -      stdvx=zeros(length(CH),1);
37 -      skewx=zeros(length(CH),1);
38 -      kurtx=zeros(length(CH),1);
39 -      dstdv=zeros(length(CH),1);
40 -      dskew=zeros(length(CH),1);
41 -      dkurt=zeros(length(CH),1);
42 -      pdfx=zeros(length(CH),histbins);
43 -      pdfy=zeros(length(CH),histbins);
44 -      dpdfx=zeros(length(CH),histbins);
45 -      dpdfy=zeros(length(CH),histbins);
46 -      diff1=zeros(histbins,1);
47 -      diff2=zeros(histbins,1);
48 -      diff3=zeros(histbins,1);
49 -      diff4=zeros(histbins,1);
```

```matlab
50
51      % Begin the loop: This loop analizes one recording and extracts all the
52      % important statistical information. This information is then stored for
53      % latter use.
54  ┌ for c=1:length(CH);
55  │       c % a visual indicator to see how fast we are looping
56  │       % Open the file
57  │       filename=[pathname,testname,sprintf('%03.0f',ID),'_',...
58          sprintf('%03.0f',CH(c)),'.bin'];
59
60      fid=fopen(filename,'r');
61      N=20*fs; % Number of datapoints = Number of secconds we wish to analize *
62      Nstart=4*(629)*fs; %Starting point (about 42 minutes in)
63      fseek(fid,Nstart,'bof'); % find the starting point in the file
64      x=fread(fid,N,'single'); % extract 20 sec of data
65      fclose(fid); % close the file
66      % Create the time axis
67      dt=1/fs;
68      t=0:dt:dt*(length(x)-1);

69      %Flip the polarity depending on the chanel
70      if CH(c)<17
71          x=-x;
72      end
73
74      stdvx(c)=std(x);        % Standard Deviation
75      skewx(c)=skewness(x);   % Skewness
76      kurtx(c)=kurtosis(x);   % kurtosis
77
78      % Perform the PDF on the function
79      [h,dx]=hist(x/stdvx(c),histbins);
80      da=dx(2)-dx(1);
81      pdfx=(1/(da*length(t)))*h;
82
83      % Interplate the PDF onto a uniform grid and store it for the 3D array
84      dxint=-5:.1:11;
85      pdfx3D(c,:)=interp1(dx,pdfx,dxint,'linear');
86
87      % Perform the first order difference
88      dir=diff(x)/da;
89
90      dstdv(c)=std(dir);        % Standard Deviation
91      dskew(c)=skewness(dir);   % Skewness
92      dkurt(c)=kurtosis(dir);   % kurtosis
93
94      % Perform the PDF on the first order difference
95      [dh,ddx]=hist(dir/dstdv(c),histbins);
96      dda=ddx(2)-ddx(1);
97      Dpdfx=(1/(dda*length(t)))*dh;
98
99      %Interplate the PDF onto a uniform grid and store it for the 3D array
100     ddxint=-90:.1:133;
101     Dpdfx3D(c,:)=interp1(ddx,Dpdfx,ddxint,'linear');
102  └ end
```

```matlab
104        %Plot the 3D PDF - data
105 -      figure
106 -      surf(dxint,Scale,log10(pdfx3D))
107 -      xlabel('Standard Deviations')
108 -      ylabel('Distance Along Radial in Nozzle Diameters');
109 -      title('log_{10}(PDF) - \it{p}(\it{t}) ORION-50');
110 -      shading interp
111 -      caxis([-6,-.1])
112 -      colorbar
113 -      view(2)
114 -      set(gcf,'position',[20,10,400,800]);
115
116        %Plot the 3D PDF - derivative
117 -      figure
118 -      surf(ddxint,Scale,log10(Dpdfx3D))
119 -      xlabel('Standard Deviations')
120 -      ylabel('Distance Along Radial in Nozzle Diameters');
121 -      title('log_{10}(PDF) - \partial\it{p}\rm{/\partial}\it{t} \rm{ORION-50}');
122 -      shading interp
123 -      caxis([-6,-.1])
124 -      colorbar
125 -      view(2)
126 -      set(gcf,'position',[20,10,400,800]);
127
128        %Plot OASPL
129 -      figure
130 -      plot(Scale,stdvx)
131 -      xlabel('Distance Along Radial in Nozzle Diameters')
132 -      ylabel('Pressure (Pa)');
133 -      title('OASPL');
134
135        %Plot skewness - data
136 -      figure
137 -      plot(Scale,skewx)

138 -      xlabel('Distance Along Radial in Nozzle Diameters')
139 -      ylabel('Skewness');
140 -      title('Skewness of the data');
141
142        % Plot kurtosis - data
143 -      figure
144 -      plot(Scale,kurtx)
145 -      xlabel('Distance Along Radial in Nozzle Diameters')
146 -      ylabel('Kurtosis');
147 -      title('Kurtosis of the data');
148
149        % Plot skewness - derivative
150 -      figure
151 -      plot(Scale,dskew)
152 -      xlabel('Distance Along Radial in Nozzle Diameters')
153 -      ylabel('Skewness');
154 -      title('Skewness of the derivative');
```

```
155
156        % Plot Kurtosis - derivative
157 -      figure
158 -      plot(Scale,dkurt)
159 -      xlabel('Distance Along Radial in Nozzle Diameters')
160 -      ylabel('Kurtosis');
161 -      title('Kurtosis of the derivative');
```

Bibliography

[1] S. McInerny, "Rocket Noise - A Review," In *AIAA 13th Aeroacoustics Confrence(October 22-24, 1990 / Tallahassee, FL)*, pp. 1–9 (1990).

[2] W. C. Horne, N. J. Burnside, J. Panda, and C.Brodell, "Measurments of Unsteady Pressures near the Plume of a Solid Rocket Motor," In *The 15th AIAA/CEAS Aeroacoustics Confrence (30th AIAA Aeroacoustics Confrence)*, pp. 1–14 (2009).

[3] L. E. Kinsler, A. R. Frey, A. B. Coppens, and J. V. Sanders, in *Fundamentals of Acoustics*, fourth ed., S. Johnson, ed., (John Wiley & sons, Inc., 111 River Street, Hoboken, NJ, 2000).

[4] M. B. Muhlestein, K. L. Gee, and J. H. Macedone, "A pedagogical demonstration of weak-shock propagation from a gas-filled balloon explosion," Journal of the Acoustical Society of America **129,** 2648 (2011).

[5] K. L. Gee, V. W. Sparrow, A. Atchley, and T. B. Gabrielson, "On the Perception of Crackle in High-Amplitude Jet Noise," AIAA **38,** 593–598 (2007).

[6] J. E. F. Williams, J. Simson, and V. J. Virchis, "'Crackle': an annoying component of jet noise," Journal of Fluid Mechanics **71,** 251–271 (1975).

[7] K. L. Gee, S. H. Swift, V. W. Sparrow, K. J. Plotkin, and J. M. Downing, "On the potental limitations of conventional sound metrics in quantifying perception of nonlinearly propagated noise," Jornal of the Acoustical Society of America **121,** EL1–EL7 (2007).

[8] S. McInerny, K. L. Gee, M. Dowing, and M. James, "Acoustical nonlinearities in aircraft flyover data," AIAA Paper (2007).

[9] B. P. Petitjean, K. Viswanathan, and D. K. McLaughlin, "Acoustic pressure waveforms measured in high speed jet noise experienceing nonlinear propagation," International Journal of Aeroacoustics **5,** 193–215 (2006).

[10] K. L. Gee, J. H. Giraud, J. D. Blotter, and S. D. Sommerfeldt, "Near-field vector intensity measurments of a small solid rocket motor," Journal of the Acoustical Society of America **128,** EL69–EL74 (2010).

[11] K. L. Gee, J. H. Giraud, J. D. Blotter, and S. D. Sommerfeldt, "Energy-Baised Acoustical Measurments of Rocket Noise," AIAA Paper (2009).

[12] T. Taylor, Bachelor of science thesis, Brigham Young University, Department of Physics and Astronomy, 2011.

Index